



Rowland, G. H., Ng, H. C., Robinson, L. F., McManus, J. F., Mohamed, K. J., & McGee, D. (2017). Investigating the use of $^{232}\text{Th}/^{230}\text{Th}$ as a dust proxy using co-located seawater and sediment samples from the low-latitude North Atlantic. *Geochimica et Cosmochimica Acta*, 214, 143-156.
<https://doi.org/10.1016/j.gca.2017.07.033>

Peer reviewed version

Link to published version (if available):
[10.1016/j.gca.2017.07.033](https://doi.org/10.1016/j.gca.2017.07.033)

[Link to publication record in Explore Bristol Research](#)
PDF-document

This is the accepted author manuscript (AAM). The final published version (version of record) is available online via Elsevier at DOI: 10.1016/j.gca.2017.07.033. Please refer to any applicable terms of use of the publisher.

University of Bristol - Explore Bristol Research

General rights

This document is made available in accordance with publisher policies. Please cite only the published version using the reference above. Full terms of use are available:
<http://www.bristol.ac.uk/pure/about/ebr-terms>

Investigating the use of $^{232}\text{Th}/^{230}\text{Th}$ as a dust proxy using co-located seawater and sediment samples from the low-latitude North Atlantic

George H. Rowland ^{a*} Hong Chin Ng ^a Laura F. Robinson ^a Jerry F. McManus ^b Kais J. Mohamed ^c David McGee ^d

^aSchool of Earth Sciences, Wills Memorial Building, University of Bristol, Bristol, BS8 1RJ, UK (*correspondence: gr1850@bristol.ac.uk)

^bLamont-Doherty Earth Observatory of Columbia University, 61 Route 9W, Palisades, New York 10964, USA

^cDepartamento Geociencias Marinas y Ordenación del Territorio, Facultad de Ciencias del Mar, Universidad de Vigo, 36310 Vigo

^dMassachusetts Institute of Technology, 45 Carleton Street, Building E25, Room 625, Cambridge, MA 02142

Abstract

The thorium isotope ratio $^{232}\text{Th}/^{230}\text{Th}$ can be measured in seawater and sediment samples, and has been used as a proxy to reconstruct lithogenic fluxes to the oceans for the modern day and the Pleistocene. There has not yet been a study testing the proxy using the $^{232}\text{Th}/^{230}\text{Th}$ ratio in seawater and the ratio recorded in the underlying sediment. In this study we use co-located core-top sediments and seawater samples from five seamount sites spanning the tropical North Atlantic to investigate the link between seawater and sediment $^{232}\text{Th}/^{230}\text{Th}$ ratios across a range of water depths. Our results indicate that a broad correlation exists between seawater and sedimentary $^{232}\text{Th}/^{230}\text{Th}$ ratios. Both seawater and sedimentary $^{232}\text{Th}/^{230}\text{Th}$ ratios record a signal consistent with decreasing lithogenic input east to west, from Africa to South America. However, calculated ^{232}Th fluxes for the core-top sediment samples indicate a strong dependence on depth, with up to a factor of ~ 4 difference from shallow (<600 m) to deep sites (>2900 m). This depth dependence is likely caused by either a deficit of ^{230}Th burial at depth compared to the production in the overlying water column, through addition of ^{232}Th , or by a combination of the two processes. By comparing seawater and sedimentary $^{232}\text{Th}/^{230}\text{Th}$ ratios we derive an apparent fractional solubility of ^{232}Th of $29 \pm 3\%$, in reasonable agreement with the upper end of existing estimates.

1 1. Introduction

2 Aeolian dust is an important but poorly quantified part of the climate system. Dust affects the
3 climate through interaction with radiation in the Earth's atmosphere and plays a part in the
4 carbon cycle by delivering key micronutrients, such as iron, to the ocean (Jickells et al.,
5 2005; Maher et al., 2010). Knowledge of present day dust fluxes to the ocean comes from
6 model simulations (Mahowald et al., 2005), direct observations (Lawrence and Neff, 2009)
7 and geochemical data (Measures et al., 2008; Hsieh et al., 2011). Model simulations provide
8 a global picture of dust fluxes to the oceans (Niedermeier et al., 2014), but rely on poorly
9 constrained parameters such as the surface properties of the dust source regions, giving rise
10 to uncertainties in simulated fluxes (Mahowald et al., 2005). Given the relative scarcity of
11 direct observations (Kohfeld and Harrison, 2001), geochemical proxy methods provide a
12 means of testing and improving these models as well as our knowledge of dust fluxes
13 (Anderson et al., 2016).

14

15 A widely used method has been the measurement of Al concentrations in the dissolved
16 phase in seawater e.g. (Measures et al., 2008). This approach draws on the fact that the
17 main supply of Al to the ocean is from continentally-derived lithogenic particles. In remote
18 parts of the ocean, dust is the main source of continental material, and so dissolution of
19 these grains leads to a measurable dissolved Al concentration that is correlated with
20 expected dust input (Hydes, 1983). However, a key difficulty in using dissolved Al to
21 reconstruct dust fluxes is in calculating a local residence time (Hsieh et al., 2011). A related
22 geochemical method that allows for the calculation of a local residence time is the combined
23 measurement of two isotopes of thorium: ^{232}Th and ^{230}Th (Hsieh et al., 2011; Hayes et al.,
24 2013).

25

26 Th-232 is a long lived (half-life = 1.4×10^{10} yrs; Holden, 1990) primordial nuclide that is found
27 in the upper continental crust at a concentration of approximately 11 ppm (Taylor and
28 McLennan, 1985). As for Al, ^{232}Th is concentrated in the continental crust, so it can be used
29 to trace lithogenic material with a continental origin. Dissolved ^{232}Th in seawater is therefore
30 assumed to be derived from the dissolution of continental detritus in seawater (Hsieh et al.,
31 2011; Hayes et al., 2013; Deng et al., 2014; Lopez et al., 2015). Given that ^{232}Th provides a
32 means of tracking the input of continental material to the ocean, the only other factor needed
33 in order to calculate a flux of dust is a timescale for ^{232}Th addition. The shorter lived isotope
34 ^{230}Th can be used to provide this timescale. Th-230 has a half life of 75,584 yrs (Cheng et
35 al., 2013), and is sourced from the radioactive decay of ^{234}U in seawater. Th-230 is
36 scavenged rapidly onto sediment particles (although the adsorbed ^{230}Th is thought to
37 maintain a reversible exchange with a pool of dissolved ^{230}Th ; Bacon and Anderson, 1982),

38 meaning that ^{230}Th has a short oceanic residence time of up to ~40 yrs (Anderson et al.,
39 1983). The residence time of ^{230}Th in seawater can be derived from measurements of ^{230}Th
40 activity in seawater combined with the known production of ^{230}Th from ^{234}U (Broecker et al.,
41 1973). Making the assumption that ^{230}Th and ^{232}Th share the same residence time, the
42 seawater dissolved ^{232}Th concentration can be combined with the ^{230}Th -derived residence
43 time, to determine a flux of dissolved ^{232}Th . Combining dissolved flux estimates with
44 estimates of the fractional solubility of ^{232}Th from continental material allows a total flux of
45 ^{232}Th to be estimated (Hsieh et al., 2011; Hayes et al., 2013; Deng et al., 2014). Estimates of
46 solubility currently account for a significant source of uncertainty in studies that estimate total
47 ^{232}Th flux from dissolved ^{232}Th fluxes (Hsieh et al., 2011; Hayes et al., 2013).

48

49 Both these isotopes of thorium have also been measured in sediments in order to estimate
50 lithogenic fluxes in the past (Pourmand et al., 2004; Anderson et al., 2006; McGee et al.,
51 2007; Winckler et al., 2008; Lam et al., 2013; Serno et al., 2014; Costa et al., 2016; Jacobel
52 et al., 2016; Kienast et al., 2016; Williams et al., 2016). In this scenario ^{232}Th measured in
53 sediments is assumed to be sourced only from the input of continental detritus (Pourmand et
54 al., 2004; Anderson et al., 2006; McGee et al., 2007). Far from ocean margins it has been
55 assumed that all ^{232}Th in the sediment (in both adsorbed and lattice-bound pools) is sourced
56 from continental aeolian dust (Anderson et al., 2006; McGee et al., 2007; Hsieh et al., 2011;
57 Hayes et al., 2013; Lopez et al., 2015).

58

59 The two thorium based methods described above both make use of the constant input of the
60 isotope ^{230}Th in order to calculate a timescale. The intense scavenging from the water
61 column leads to efficient removal of ^{230}Th . If the flux of ^{230}Th to the sediment is assumed to
62 be equal to the production flux of ^{230}Th in the overlying water column (β , $\sim 0.0267 \text{ dpm m}^{-3} \text{ yr}^{-1}$;
63 Francois et al., 2004), then the $^{230}\text{Th}_{\text{xs}}$ activity concentration (in dpm g^{-1} , where 'xs'
64 denotes excess ^{230}Th that is not supported by ^{234}U decay in the sediment) in the sediment is
65 a function of the sediment flux to the seafloor. Therefore measurement of $^{230}\text{Th}_{\text{xs}}$ in the
66 sediment allows vertical mass fluxes at a given water depth (z , in metres) to be calculated
67 (Equation 1). This method of calculating vertical sediment fluxes is termed ' ^{230}Th
68 normalisation' (Francois et al., 2004). Early studies used this method to calculate lithogenic
69 fluxes in the Atlantic (Francois and Bacon, 1991). By combining the sediment mass flux
70 calculated by ^{230}Th normalisation with the fractional concentration of ^{232}Th in the sediment (in
71 $\mu\text{g g}^{-1}$), a vertical flux of ^{232}Th (in $\mu\text{g m}^{-2} \text{ yr}^{-1}$) to the seafloor can be calculated (Equation 2). If
72 the ^{232}Th concentration in lithogenic material is known, then an estimate of the lithogenic flux
73 can be made (e.g. McGee et al., 2007). Recently it has been suggested that a concentration
74 of 14 ppm is appropriate for estimating dust fluxes using this method for most locations

75 receiving fine-grained dust (McGee et al., 2016). If the $^{232}\text{Th}/^{230}\text{Th}$ ratio of the adsorbed
76 phase of thorium is known ($(^{232}\text{Th}/^{230}\text{Th})_{\text{Ads}}$ in $\mu\text{g dpm}^{-1}$), an adsorbed flux of ^{232}Th can also
77 be calculated (Robinson et al., 2008; Equation 3). This ‘adsorbed’ pool of thorium can be
78 accessed by leaching sediments without dissolving the ^{232}Th bearing lithogenic phases
79 (Robinson et al., 2008).

80

81 Equation 1. Sedimentary mass flux = $\beta * z / ^{230}\text{Th}_{\text{xs}}$

82

83 Equation 2. ^{232}Th flux = Sedimentary mass flux * ^{232}Th

84

85 Equation 3. Adsorbed ^{232}Th flux = $(^{232}\text{Th}/^{230}\text{Th})_{\text{Ads}} * \beta * z$

86

87 Determination of ^{232}Th and ^{230}Th in ocean sediments and seawater therefore has the
88 potential to provide the basis for estimating fluxes of continental material (both in the past
89 and in modern times). However, there has not yet been a study that combines
90 measurements of ^{232}Th and ^{230}Th in core-top sediments with co-located seawater samples.

91

92 In this study, we assess the relationship between modern seawater and core-top
93 sedimentary $^{232}\text{Th}/^{230}\text{Th}$ ratios in the tropical North Atlantic Ocean. This area is, in part,
94 beneath the path of dust emitted from the largest dust source on Earth, the Sahara Desert
95 (Goudie and Middleton, 2001; Cakmur et al., 2006). We present measured $^{232}\text{Th}/^{230}\text{Th}$ ratios
96 and concentrations in core-top sediments and seawater samples, and compare how the
97 values vary across the basin as well as with water depth. We calculate ^{230}Th -normalised
98 mass fluxes and ^{232}Th fluxes for our sample sites and investigate the spatial and vertical
99 variability of these parameters. We also estimate the apparent fractional solubility of ^{232}Th , a
100 parameter that is poorly constrained but essential for calculating total fluxes of ^{232}Th from
101 dissolved ^{232}Th concentrations in seawater (Hsieh et al., 2011).

102

103 2. Study area, sampling strategy and sample collection

104 Core-top sediments were collected from five sites from the JC094 TROPICS (TRacing
105 Oceanic Processes using Corals and Sediments) cruise aboard RRS *James Cook* during
106 October and November 2013 (Figure 1; Robinson, 2014). The sampling strategy exploited
107 extremes in bathymetry to provide core-top sediment samples from 570 m to 4565 m. The
108 five sampling locations are named based on their proximity to major bathymetric features
109 (Figure 1). The ‘Carter’ and ‘Knipovich’ sites are seamounts in the eastern basin, ‘Vema’
110 makes up part of the Vema fracture zone on the mid-Atlantic ridge, whilst ‘Vayda’ and
111 ‘Gramberg’ are two seamounts from the Researchers Seamounts in the western basin. The

112 targeting of bathymetric highs spanning the Atlantic allows approximate sedimentary depth
113 transects to be constructed at each location.

114

115 Short mega-core and remotely operated vehicle (ROV) push-core sampling equipment were
116 used in order to ensure the best possible preservation of sediment core-tops. In one
117 instance box-core apparatus was used to collect a core-top sample. Core samples were
118 stored at 5°C. Radiocarbon ages for all core-top sediments (derived from planktonic
119 foraminifera) indicate that they are between 1000 and 8870 yr BP, with an average age of
120 ~4300 yr BP (supplementary information).

121

122 Seawater samples (~5 L) were collected close to the core-top sample sites by Niskin bottles
123 on the CTD rosette, the ROV, or mounted on the mega-core frame and were filtered through
124 acropak (0.2 µm) filters into acid-cleaned plastic jerry cans, and acidified on the day of
125 collection with 5ml of concentrated ultrapure hydrochloric acid.

126

127 3. Analytical procedures

128 3.1 Sediment dissolution laboratory procedure

129 Aliquots of dried sediment (~0.5 g) were taken from the top 1 cm of each core and then
130 mechanically homogenised using an agate mortar and pestle. Approximately 0.1 g aliquots
131 of the homogenised sediment were weighed out and spiked with a mixed ²³⁶U and ²²⁹Th
132 spike. The samples were dissolved in 7 ml 14 N HNO₃, 3 ml 28 N HF and 2 ml 11.6 N
133 HClO₄. The samples were passed through columns containing 1.5 ml of an anion exchange
134 resin (Eichrom 1-X8 100-200 mesh) in order to separate U and Th. The Th fraction was
135 further purified through a second anion exchange column. Th separates were refluxed with
136 HClO₄ and H₂O₂ to eliminate organic matter, and the U separates were refluxed with H₂O₂
137 only. Two procedural blanks were analysed with each batch of 8 samples.

138

139 3.2 Sediment leaching laboratory procedure

140 The method used broadly followed that of Robinson et al. (2008). Approximately 0.1 g of
141 homogenised sediment (from the same aliquots used in the total dissolution procedure) from
142 the Carter Seamount samples were leached in 3 N HCl for 20 minutes with ultrasonication.
143 The samples were then centrifuged, and the supernatant liquid was pipetted from the
144 centrifuge tubes. The supernatant liquid was then weighed and spiked with both ²³⁶U and
145 ²²⁹Th spikes. The samples were then passed through anion exchange resin as for the total
146 dissolution procedure.

147

148 3.3 Seawater analysis

149 Seawater samples were spiked with ^{229}Th and ^{236}U and allowed to equilibrate before being
150 precipitated with ammonium hydroxide to a pH of 7.5-8. The supernatant was removed using
151 a peristaltic pump, and the precipitate dissolved in concentrated hydrochloric acid, before
152 separation of Th and U isotopes using anion exchange column chromatography. The
153 methods for the separation of Th and U isotopes follow those set out by Auro et al. (2012).

154 155 3.4 Mass spectrometric analysis

156 Mass spectrometry was carried out using a Thermo Scientific Neptune multi-collector
157 inductively coupled plasma mass spectrometer (MC-ICP-MS; Auro et al., 2012; Chen et al.,
158 2015). A standard bracketing method was used in order to apply corrections for mass bias
159 and ion counter yield; in-house thorium (Th-SGS) and the uranium standards U-112a were
160 used as bracketing standards. Sample uptake was through a CETAC Aridus desolvating
161 nebulizer. Measurement at half masses (230.5, 229.5, 228.5) accounted for the tailing effect
162 of ^{232}Th . The same procedure was applied to U measurements at half masses 234.5 and
163 233.5 to account for ^{238}U tailing. An exponential tail profile was assumed for interpolation
164 between half masses (Hoffman et al., 2007). The size of the ^{232}Th tailing correction on the
165 ^{230}Th beam was <2% of the ^{230}Th beam for nearly all samples (abundance sensitivity of ~0.5
166 ppm of the ^{232}Th beam intensity at mass 230). The average sizes of full procedural blanks
167 from three separate batches of total dissolution of sediment analyses (with approximate
168 fractional size of blanks compared to the sample signal shown in parentheses) are: 29 ± 6.3
169 $\text{pg } ^{232}\text{Th}$ (~0.015 %), $4.3 \pm 1.5 \text{ fg } ^{230}\text{Th}$ (~0.054 %), $70 \pm 120 \text{ pg } ^{238}\text{U}$ (~<0.5 %), $42 \pm 7.0 \text{ fg}$
170 ^{234}U (~1.3 %), (uncertainties are given as 2 standard errors from the mean). The uncertainty
171 of the ^{238}U blank reflects the fact that one analysis had a much higher blank than the other
172 two (but still <0.5% of sample signals).

173
174 Procedural blanks from the leaching procedure are $2.4 \pm 0.63 \text{ pg } ^{232}\text{Th}$ (~0.024%), $0.01 \pm$
175 $0.027 \text{ fg } ^{230}\text{Th}$ (~0.004%), and U blanks were negligible. The average procedural blanks from
176 two separate seawater procedures are $6.8 \pm 2.4 \text{ pg } ^{232}\text{Th}$ (~1-5%, except for two samples
177 with lower ^{232}Th concentration which are ~10%) and $0.6 \pm 0.5 \text{ fg } ^{230}\text{Th}$ (~0.2-4%).

178 179 3.5 Carbonate content determination

180 Carbonate contents of the sediments were determined using a Carlo Erba NC2500
181 elemental analyser at the University of Liverpool. Small aliquots of sediment were analysed
182 for total carbon, exposed to HCl fumes overnight in order to digest the carbonate fraction,
183 and were then analysed for organic carbon. The carbonate content of the sediment was
184 calculated from the difference between the total carbon and organic carbon. The aliquots of

185 sediment were run in duplicate, with the average uncertainty of all 18 samples $\sim \pm 0.5\%$
186 (based on 2 standard deviations from the mean; supplementary information).

187

188 3.6 Opal content determination

189 Biogenic opal analysis was carried out at the University of Bristol broadly following the
190 procedures of Mortlock and Froelich (1989). About 50 mg of mechanically homogenised dry
191 sediment was exposed to 5 ml of 1 N HCl and 5 ml of 10% H₂O₂ and agitated in an ultrasonic
192 bath to remove carbonates and organics. Samples were centrifuged in deionised water, and
193 the supernatants removed before drying of the residual sediment in an oven. The biogenic
194 opal fraction was leached from the dry sediment by adding 40 ml 2 M Na₂CO₃ and heating in
195 a water bath at 80°C for 5 hours. Duplicates of each sample were prepared by pipetting off
196 two separate aliquots from the supernatant. Opal contents were determined using a Hach
197 DR3900 spectrophotometer following the molybdate-blue spectrophotometry procedures and
198 reagents recommended by the Hach Company. Prior to sample analysis, instrumental
199 baseline was determined and internally corrected for by measuring a blank.

200

201 4. Results

202 4.1 Filtered seawater ²³²Th and ²³⁰Th

203 Th-230 concentrations range from 4 to 15 fg kg⁻¹ (Figure 2a; supplementary information) in
204 good agreement with previously reported nearby data (Moran et al., 2002). Above ~2500 m
205 depth at Carter, Knipvoch and Vema, seawater ²³⁰Th concentrations show an approximately
206 linear increase with depth, but below ~2500 m the rate of concentration increase at Carter
207 and Knipovich profiles decreases (Figure 2a). Th-230 concentrations from Vayda do not
208 show any obvious trend with depth (Figure 2a). Th-232 concentrations from all sites are in
209 broad agreement with previous measurements at nearby stations (Moran et al., 2002). Th-
210 232 concentrations do not show any obvious overall trends with depth and range from 14 to
211 97 pg kg⁻¹ (Figure 2b; supplementary information). Seawater ²³²Th/²³⁰Th atom ratios range
212 from 3400 to 14500 (Figure 3; supplementary information), also in broad agreement with
213 previously reported ²³²Th/²³⁰Th ratios from nearby stations (Moran et al., 2002). In general,
214 ratios decrease with depth and are higher at eastern sites compared to western sites across
215 the range of depths sampled (Figure 3).

216

217 4.2 Core-top sediment ²³²Th and ²³⁰Th

218 Sedimentary ²³⁰Th_{xs} concentrations increase with depth at all seamounts with a range of 1.1
219 to 12.6 dpm g⁻¹. Vayda seamount (in the West) shows the highest values at depth, whilst the
220 concentrations across all stations converge at shallower depths (Figure 2c).

221

222 Th-232 concentrations in core-top sediments range from 0.80 to 5.9 $\mu\text{g g}^{-1}$ and increase with
223 depth at all seamount locations (Figure 2d). The magnitude of ^{232}Th concentration change
224 with depth is a factor of 5 at the Carter seamount (in the East). The trends in ^{232}Th and
225 $^{230}\text{Th}_{\text{xs}}$ concentration with depth above about 3000 m are close to linear, but below 3000 m
226 the rate of concentration change increases.

227

228 Total sediment digest $^{232}\text{Th}/^{230}\text{Th}_{\text{xs}}$ atom ratios for all seamounts range from 13,000 to
229 43,000 (Figure 3). At all locations the ratios show an overall decrease from the shallowest to
230 deepest sample sites. However, there is variation at intermediate depths notably at Carter
231 and Vema which show a mid-depth minimum and a mid-depth maximum respectively.
232 Generally, ratios are lower in the West and higher in the East.

233

234 Leached core-top sediment $^{232}\text{Th}/^{230}\text{Th}$ atomic ratios generally decrease with depth, with a
235 range of 8600 to 25700 (Figure 3). The leached ($^{234}\text{U}/^{238}\text{U}$) activity ratios (supplementary
236 information) are close to the seawater value of 1.147 (Robinson et al., 2004).

237

238 4.3 Carbonate and opal contents

239 The carbonate content ranges from 58-90 %. The carbonate content typically decreases with
240 depth, and the rate of carbonate change with depth increases at depths >3000 m (Figure
241 4a).

242 The opal content of the sediment ranges from 0.6-3.4 %. The Opal content of the sediments
243 increase with depth and show a strong negative correlation with carbonate content ($R^2=0.91$;
244 supplementary information).

245

246 4.4 ^{230}Th -normalised sedimentary fluxes

247 Calculated mass fluxes range from 8 to 22 $\text{g m}^{-2} \text{yr}^{-1}$ (Figure 4b). Mass fluxes are variable
248 down to 2000 m, and at greater depths mass fluxes then decrease with depth. There is a
249 broad trend of decreasing maximum mass flux from eastern to western sites.

250

251 Calculated ^{232}Th fluxes range from 9 to 63 $\mu\text{g m}^{-2} \text{yr}^{-1}$ (Figure 4c). An increase in ^{232}Th flux
252 with depth is seen at each sample site, ranging in magnitude from a factor of ~4.3 at Vema
253 to a factor of ~1.2 at Gramberg. The increase at Carter Seamount is factor of ~3.6 over the
254 entire depth transect, and ~1.4 between 2719 and 4565 m. At depths >~2000 m a broad
255 trend in ^{232}Th fluxes can be seen between sample locations, with higher fluxes in the east
256 (e.g. Carter and Knipovich) and lower fluxes in the west (Vayda and Gramberg; Figure 4c).

257

258 Calculated ^{232}Th fluxes from the leached Carter sediment range from 9 to 23 $\mu\text{g m}^{-2} \text{yr}^{-1}$.
259 There is a general trend, approximately doubling with depth, that correlates strongly with
260 total ^{232}Th fluxes from Carter ($R^2 = 0.99$).

261

262 5. Discussion

263 5.1 ^{232}Th and ^{230}Th in seawater and sediment

264 The new seawater and sedimentary Th concentration profiles and $^{232}\text{Th}/^{230}\text{Th}$ ratios are
265 generally in line with expectations, based on the findings of previous studies (Moran et al.,
266 2002; Robinson et al., 2008; Hsieh et al., 2011; Deng et al., 2014). At four sites the ^{230}Th in
267 seawater increases with depth, consistent with reversible scavenging (Bacon and Anderson,
268 1982). The departure from linear increases in ^{230}Th concentration below ~2500 m recorded
269 at Carter, Knipovich and Vema is consistent with previous observations in the Atlantic
270 (Marchal et al., 2007). This feature may be explained by ventilation of deep waters (Moran et
271 al., 2002; Marchal; et al., 2007; Hayes et al., 2015a), enhanced scavenging in deep waters
272 due to a bottom scavenging effect (Okubo et al., 2012), or potentially by vertical variations in
273 the rates of adsorption versus desorption (Lerner et al., 2016). An exception to this typical
274 profile is seen at Vayda, where the ^{230}Th (and ^{232}Th) concentration in seawater decreases at
275 mid-depth. Given the deviation from the expected profiles of both isotopes and the location
276 of the Vayda site relatively close to the mid-Atlantic ridge, the presence of a hydrothermal
277 plume could offer an explanation for the trends seen at this site. This interpretation is
278 supported by previous studies demonstrating the likelihood of a number of undiscovered
279 hydrothermal vents on the ridge (Beaulieu et al., 2015) and that hydrothermal plumes
280 strongly scavenge thorium in the North Atlantic (Hayes et al., 2015b). The profiles of ^{232}Th in
281 seawater are broadly consistent with a surface source of ^{232}Th (i.e. dust) followed by a
282 reversible scavenging behaviour. The exact profile would depend on the relative rates of
283 particle sinking, adsorption and desorption (Lerner et al., 2016), but we observed profiles
284 with no clear vertical trends. The $^{232}\text{Th}/^{230}\text{Th}$ ratios generally decrease with depth in all
285 phases (seawater, total digestions of sediments and sediment leachates), as expected from
286 in-situ production and subsequent reversible scavenging behaviour of ^{230}Th and the
287 approximately constant vertical profiles of ^{232}Th .

288

289 Leaching of sediments can help to constrain the adsorbed pool of thorium bound to sediment
290 surfaces. The ratio of adsorbed $^{232}\text{Th}/^{230}\text{Th}$ is expected to be the same as that of the
291 dissolved thorium in the water column (Robinson et al., 2008). The $^{232}\text{Th}/^{230}\text{Th}$ ratios of
292 leached sediment samples from Carter show a positive correlation with co-located seawater
293 samples ($R^2 = 0.81$), but with systematically slightly higher values (Figure 3). However, the
294 leached $^{232}\text{Th}/^{230}\text{Th}$ ratios correlate even more strongly with those of the total sediment

295 digestions ($R^2=0.86$). This correlation along with the elevation of the leachate ratios (relative
296 to the seawater ratios) are most simply explained by release of some lattice bound ^{232}Th that
297 is accessed by the leaching procedure. Although Robinson et al. (2008) showed little change
298 in $^{232}\text{Th}/^{230}\text{Th}$ when leaching in HCl ranging in concentration from 0.1-6 N, the liberation of
299 extra ^{232}Th by 3 N HCl does provide a plausible explanation for the elevated leached ratios
300 presented here.

301

302

303 5.2 ^{230}Th -normalised flux trends with location

304 Mass fluxes at depths ~500-2000 m do not show any coherent spatial trends, however for
305 samples at depths below ~2000 m there is a broad pattern of higher ^{230}Th -normalised mass
306 fluxes in the east compared to the west (Figure 4b). Although subtle, this gradient is
307 consistent with higher biological productivity in the east (as indicated by chlorophyll
308 concentrations in surface waters, Wang et al., 2013).

309

310 Continental material to the low latitude Atlantic is expected to be supplied from Saharan dust
311 (Ridley et al., 2012), with higher continental inputs generally expected at sites in the east
312 (e.g. Mahowald et al., 2005). Indeed, increasing seawater $^{232}\text{Th}/^{230}\text{Th}$ ratios at sites
313 underlying the Saharan dust plume have previously been identified from a latitudinal transect
314 at approximately 30°W (Hsieh et al., 2011). With scavenging of all of the ^{230}Th produced in-
315 situ to the sediment we would expect the $^{232}\text{Th}/^{230}\text{Th}$ ratios (and ^{232}Th fluxes) to be higher in
316 the east than the west. As with the ^{230}Th -normalised mass fluxes, we do observe a broad
317 east to west trend in maximum ^{232}Th fluxes (Figure 4c). At our sites, seasonal variations in
318 dust deposition may also play a role in controlling the spatial patterns of dust flux recorded.
319 For example, Carter and Knipovich lie under the approximate latitude of the winter dust
320 plume, whereas Vayda and Gramberg (further north) lie in the range of summer dust and
321 Vema could receive dust from both summer and winter dust plumes (Eglinton et al., 2002).
322 In addition, it is possible that sites close to the basin margins may receive some direct
323 contribution of lithogenic material from the continents (Francois and Bacon, 1991). However,
324 even with these potential complications, we do see an overall decrease in $^{232}\text{Th}/^{230}\text{Th}$ ratios
325 and ^{232}Th fluxes moving from sites in the east to the west, both in seawater and in the
326 sediment broadly in line with the expected trend from Saharan dust inputs (Figure 3).

327

328 5.3 ^{230}Th -normalised flux trends with depth

329 With the complete scavenging of all the ^{230}Th produced by in-situ decay of dissolved ^{234}U
330 and no dissolution of sediment, the vertical mass fluxes at any given location should be the
331 same, independent of water depth. However, the dissolution of carbonate material (De

332 Villiers, 2005) leads to a reduction in the preserved vertical mass flux with increasing water
333 depth, a feature that is most obvious at water depths greater than 2000 m (Francois et al.,
334 1990; Henderson and Anderson, 2003; Francois et al., 2004; Figure 4b).

335

336 A more surprising result was the increase in ^{232}Th fluxes with depth. Given the prevailing
337 view that in remote parts of the ocean, dust addition at the surface is the dominant
338 mechanism that delivers ^{232}Th to the seafloor, our observation of large increases in apparent
339 ^{232}Th fluxes with water depth at all locations sampled in this study is unexpected. No clear
340 trends in ^{232}Th flux with sample age are recognised, and the exclusion of ^{232}Th flux data from
341 samples $>\sim 5$ ka does not alter the overall trends of ^{232}Th flux with depth rendering an age
342 bias unlikely (Figure S1). Leached ^{232}Th fluxes were also calculated to investigate whether
343 the trend of increasing flux with depth extends to the adsorbed fraction of ^{232}Th . There is a
344 significant increase in adsorbed flux with depth, but the smaller magnitude of this change, in
345 comparison to total ^{232}Th fluxes, suggests that the adsorbed fraction is less affected by the
346 processes that produce the apparent increases in total ^{232}Th flux (supplementary Figure S2).
347 The proportion of ^{232}Th that is in the adsorbed phase can be estimated from supplementary
348 Figure S2. Applying the method outlined by Hsieh et al. (2011) to our seawater data
349 indicates dissolved fluxes of ^{232}Th increasing by a factor of about 2 from shallow to deep
350 (supplementary information). The elevated dissolved ^{232}Th fluxes at depth could imply an
351 additional source of dissolved ^{232}Th at depth. For example, continued dissolution of dust
352 settling through the water column, dissolution of re-suspended sediment from the seamount,
353 or alternatively lateral advection of high ^{232}Th bearing waters from the distant continental
354 margins (Roy-Barman, 2009; Hayes et al., 2013). However, the trend of increasing ^{232}Th flux
355 pervades the adsorbed, dissolved and lattice bound pools of ^{232}Th , so a mechanism that can
356 explain all of these observations is required.

357

358

359 Our observation of increasing ^{232}Th fluxes with depth is not unique. For example, increasing
360 dissolved ^{232}Th fluxes with depth (from seawater) have previously been noted in the North
361 Pacific (Hayes et al., 2013), and a previous study that reconstructed terrestrial fluxes into the
362 tropical Atlantic using ^{230}Th -normalisation also recorded increases in ^{232}Th and mass fluxes
363 with depth at the Sierra Leone Rise and Ceara Rise (Francois and Bacon, 1991; Figure 4).
364 The ^{232}Th fluxes at the Ceara Rise are elevated compared to the highest values presented in
365 this study most likely explained by the proximity of the Ceara Rise to the South American
366 continent and the Amazon River (Francois and Bacon, 1991). Francois and Bacon pointed
367 towards the greatest increases in terrestrial fluxes with depth during the last deglacial period
368 to the mid-Holocene. They suggested that variations in the exposure of continental shelves

369 during periods of low sea-level could have led to more continental material being delivered to
370 the shelf edge from rivers such as the Amazon. They also suggested that resuspension of
371 the slope sediments by western boundary currents could have led to increased fluxes of
372 terrigenous material at depths >2800 m. Recent studies in the Atlantic do find some
373 evidence for nepheloid layers at the ocean margins (Hayes et al., 2015a; Lam et al., 2015),
374 but there is no clear evidence that they are consistent basin-wide features at the present day
375 that could explain our observations.

376
377

378 If ^{232}Th fluxes accurately reflect continental inputs, they imply that greater than a factor of
379 three times more continental material is supplied to the deep ocean compared to the shallow
380 ocean at Carter Seamount, and over a factor of four at Vema. The increasing fluxes of ^{232}Th
381 with depth cannot result from dust addition to the surface ocean and vertical sinking if our
382 assumptions about ^{230}Th scavenging are correct. In order for ^{230}Th -normalised ^{232}Th fluxes to
383 increase with depth, the $^{232}\text{Th}/^{230}\text{Th}$ ratio (from which fluxes are derived) must be higher at
384 increasing depths than is expected from a linear increase of ^{230}Th and a constant vertical
385 supply of ^{232}Th . In the following section we discuss three possible mechanisms that may lead
386 to elevated $^{232}\text{Th}/^{230}\text{Th}$ ratios at depth and therefore explain the observed ^{232}Th flux trends:
387 a) down slope transport of sediment with high $^{232}\text{Th}/^{230}\text{Th}$ or winnowing of fine sediments b)
388 advection of ^{230}Th or ^{232}Th in the water column, c) dissolution of carbonate sediment and
389 associated loss of ^{230}Th from the sediment.

390
391
392

393 5.3.1 Sediment transport

394 The redistribution of sediment of the seafloor is one of the drivers for the application of ^{230}Th
395 normalisation to calculate vertical mass fluxes, as many sites are subject to significant lateral
396 winnowing or focussing of sediment at the seafloor (Francois et al., 2004; Marcantonio et al.,
397 2014). Sediment deposited at seamounts and other bathymetric features on the seafloor
398 may be subject to down-slope redistribution driven by gravity (Stanley and Taylor, 1977).
399 Indeed, the potential importance of internal tides for re-suspending sediment on seamounts
400 with specific slope criticality (Peine et al., 2009) could provide a potential mechanism for the
401 redistribution of sediment after deposition. In addition the presence of pronounced benthic
402 nepheloid layers has been identified in parts of the Atlantic, highlighting the re-suspension
403 and potential movement of fine sediments (McCave, 1986; Lam et al., 2015).

404

405 A mechanism that would increase the ratio of $^{232}\text{Th}/^{230}\text{Th}$ with depth (relative to a constant
406 input of continental material at the surface and the expected increase in $^{230}\text{Th}_{\text{xs}}$ from
407 reversible scavenging), is the down-slope transport of sediment with high $^{232}\text{Th}/^{230}\text{Th}$ from
408 shallow depths. Erosion and advection of aged sediment would also contribute to high
409 $^{232}\text{Th}/^{230}\text{Th}$ due to decay of initial $^{230}\text{Th}_{\text{xs}}$. Below 2000m, there is an approximately linear
410 systematic increase in ^{232}Th flux seen at our sample sites, so the amount of addition of
411 sediment with elevated $^{232}\text{Th}/^{230}\text{Th}$ would have to be a systematic process and at each
412 seamount and across a large depth range. For this mechanism to be a viable explanation, it
413 is required that the adsorbed ^{230}Th on the sediment that is transported down slope does not
414 re-equilibrate with the surrounding water. Francois et al. (1990) modelled this process,
415 concluding that downslope transport could lead to an over-estimate in ^{230}Th -normalised
416 mass fluxes of ~10% at depth. However, other studies have concluded that focused
417 sediment can indeed re-equilibrate with dissolved ^{230}Th at the water depth at which the
418 sediment is re-deposited (Thomson et al., 1993; Thomson et al., 1999; Thomson et al.,
419 2006). If re-equilibration does occur relatively rapidly (Bacon and Anderson, 1982; Thomson
420 et al., 2006; Thomas et al., 2006), then a relatively fast mode of transport, such as a mass
421 flow, would be required to cause the observed trends in ^{232}Th fluxes (i.e. faster than the re-
422 equilibration timescale of Th). This interpretation relies on a continuous increase in ^{230}Th
423 with depth in seawater.

424

425 A second transport mechanism may relate to the preferential movement of fine-grained
426 sediment. Fine-grained sediments can be winnowed or focussed, depending on the
427 sedimentary setting. It has been shown that fine-grained sediment accounts for a
428 disproportionate amount of adsorbed $^{230}\text{Th}_{\text{xs}}$, and can be winnowed away, leading to
429 potential biases in recorded ^{230}Th -normalised fluxes of sedimentary constituents in the
430 coarse residual fraction (Kretschmer et al., 2010; McGee et al., 2010; Marcantonio et al.,
431 2014). A consequence of such winnowing would be that the calculated ^{230}Th -normalised
432 mass fluxes at our sample sites are in fact overestimated (Marcantonio et al, 2014). Recent
433 studies argue that where terrestrial material is also dominantly in the fine fraction, fluxes of
434 this component should not be biased by winnowing (Marcantonio et al., 2014; Costa and
435 McManus, 2017), and so this mechanism for increasing apparent ^{230}Th -normalised ^{232}Th
436 fluxes seems unlikely. Indeed, it has been shown that ^{232}Th is also enriched in the fine
437 fraction of lithogenic sediments (Kretschmer et al., 2010; McGee et al., 2016). The potential
438 for this mechanism to cause the observed changes in $^{232}\text{Th}/^{230}\text{Th}$ ratio would depend on one
439 isotope being substantially more enriched than the other in the fine fraction.

440

441 It is not clear from the isotope data whether physical transport of sediment could cause the
442 apparent increase in ^{232}Th flux with depth. The ^{230}Th -normalised detrital fluxes calculated
443 using the residual mass of sediment, after removing carbonate, organic carbon and opal,
444 also increase with depth (Figure 4d; Francois et al., 1990; Francois and Bacon, 1991).
445 However, the magnitude of detrital flux increases is ~15-40% lower than the ^{232}Th flux
446 increases. This result suggests that addition of ^{232}Th rich material (e.g. fine sediment
447 associated with nepheloid layers) may be a viable mechanism to increase $^{232}\text{Th}/^{230}\text{Th}$ ratios
448 at depth. The average concentration of ^{232}Th in the detrital material from the samples is 12.1
449 $\pm 0.9 \mu\text{g g}^{-1}$ (2 S.E.; supplementary data), lower than the $14 \pm 1 \mu\text{g g}^{-1}$ value recommended
450 by McGee et al. (2016) for dust flux reconstructions at locations distal to the source. The
451 McGee et al. concentration is based on the $<5 \mu\text{m}$ size fraction of dust, which typically has a
452 higher concentration of ^{232}Th than the larger size fractions (e.g. Castillo et al., 2008). The
453 presence of any lithogenic material $>5 \mu\text{m}$ could lead to the lower concentration of ^{232}Th in
454 our samples. This is plausible for at least some of our sample sites given that sediment traps
455 close to the Carter site have recorded mean spherical equivalent grain sizes of up to $17 \mu\text{m}$
456 (Ratmeyer et al., 1999).

457

458 Alternatively, the higher than expected ^{232}Th fluxes at depth could point towards limitations
459 in assumptions associated with ^{230}Th normalisation, rather than the systematics of lattice
460 bound ^{232}Th , as discussed in the following sections.

461

462 5.2.2 Advection of ^{230}Th and ^{232}Th in the water column

463 The ^{230}Th -normalisation method relies on the assumption that the scavenged flux of ^{230}Th is
464 equal to the production flux of ^{230}Th from the decay of ^{234}U in the water column (calculated
465 using the uranium activity concentration and water depth). However, if ^{230}Th is advected
466 away from the deep Atlantic (Moran et al., 2002; Hayes et al., 2015a), then this assumption
467 may become compromised (Henderson et al., 1999). Advection of ^{230}Th has been
468 demonstrated in the deep Atlantic by Moran et al. (2002). However, Deng et al. (2014) show
469 that even relatively large changes in the concentration of dissolved ^{230}Th of up to 50% in the
470 South Atlantic (imposed by enhanced bottom scavenging) lead to changes in the flux of
471 ^{230}Th to the underlying sediment of less than 0.1%.

472

473 Far from other sources of lithogenic material such as rivers, the dissolved stock of ^{232}Th in
474 the water column is generally thought to be controlled by the addition of windblown dust to
475 the ocean (Hsieh et al., 2011; Singh et al., 2013; Hayes et al., 2013; Okubo et al., 2013;
476 Deng et al., 2014; Hayes et al., 2015c; Lopez et al., 2015). However, other studies have
477 highlighted the importance of riverine sources of continental material, and the possible

478 transport of slope sediments in nepheloid layers (Francois and Bacon, 1991). In places,
479 elevated seawater ^{232}Th concentrations, in the North Atlantic for example, are thought to be
480 due to the presence of specific water masses, implying that advection of ^{232}Th can control
481 ^{232}Th profiles (Hsieh et al., 2011). Indeed, it has been suggested, through the use of
482 modelling, that dissolved ^{232}Th in the water column can be influenced by the advection of
483 water masses from continental margins (Roy-Barman, 2009). Our results from seawater
484 samples indicate that windblown dust probably does have a control on the dissolved
485 concentration of ^{232}Th . However, we cannot be sure that the entire inventory of ^{232}Th in the
486 water column is derived entirely from the surface addition of dust and one-dimensional
487 vertical sinking. Indeed, in an area subject to strong lateral advection such as the Atlantic
488 ^{232}Th could be advected as has been shown for ^{230}Th (Moran et al., 2002). Unfortunately, the
489 lack of clear systematic trends with depth in our dissolved ^{232}Th data make the identification
490 of these processes difficult. With the advent of higher resolution data such as those from the
491 GEOTRACES programme (e.g. Hayes et al., 2015a), the roles played by these processes
492 may become clearer.

493

494 5.3.3 Carbonate dissolution and ^{230}Th loss

495 With post depositional carbonate dissolution (e.g. De Villiers, 2005), we expect the activity
496 concentration of ^{230}Th in the sediment to increase with a preserved ^{230}Th -normalised mass
497 flux decreasing accordingly if ^{230}Th is re-adsorbed entirely to the remaining sediment after
498 dissolution (Henderson and Anderson, 2003; Francois et al., 2004). However, if some (or all)
499 of the ^{230}Th associated with the dissolving sediment is not re-adsorbed to the remaining
500 sediment, and there is minimal ^{232}Th in the carbonate, then dissolution may provide a
501 mechanism that could change sedimentary $^{232}\text{Th}/^{230}\text{Th}$ ratios with depth. In this scenario the
502 concentration of ^{230}Th will be reduced compared to complete re-adsorption, and the
503 preserved ^{230}Th -normalised mass flux will be larger than the case where all of the ^{230}Th is
504 retained. To test this idea we compare the extent of CaCO_3 dissolution (as also investigated
505 by Francois et al., 1990) with the change in ^{232}Th and mass fluxes with depth. We use data
506 from 2000 to > 4000m water depth at Carter, Knipovich and Vayda Seamounts which have
507 the best resolved depth transects and clear trends in mass flux and ^{232}Th flux with depth.

508

509 We can calculate F , the proportion of the sediment remaining after dissolution at a depth >
510 4000 m, assuming that the sediment is a binary mixture of non-dissolving lithogenic
511 sediment and CaCO_3 and using a reference carbonate concentration in the depth interval
512 between ~2000 and 3000 m (supplementary information). This model assumes that changes
513 in carbonate content are due to the dissolution of carbonate, rather than the addition of
514 lithogenic material (i.e. that focussing is not occurring at the sites). F is 32%, 49% and 45%

515 at the three sites Carter, Knipovich and Vayda respectively. We can then compare these F
516 values to the change in preserved ^{230}Th -normalised mass flux over the same depth interval
517 (supplementary information). The proportion of ^{230}Th -normalised mass fluxes remaining at
518 depth for the same sites are 62%, 65% and 63% at the same three sites. The ^{230}Th -
519 normalised mass fluxes are larger than expected from the observed dissolution of carbonate,
520 implying that the $^{230}\text{Th}_{\text{xs}}$ concentration in the sediments is lower than expected if the only
521 factor in changing the $^{230}\text{Th}_{\text{xs}}$ concentration were the dissolution of sediment. From this
522 comparison 48%, 26% and 15% of the ^{230}Th must be lost from the sediment at Carter,
523 Knipovich and Vayda respectively in order to explain the discrepancy between the fraction of
524 sediment remaining and the fraction of ^{230}Th -normalised mass fluxes remaining at depth.

525

526 The same amount of ^{230}Th loss that may cause higher than predicted ^{230}Th -normalised mass
527 fluxes should also be able to explain the coincident increase in the apparent ^{232}Th flux
528 increase with depth. Assuming that there is no ^{232}Th in carbonate, the amount of ^{230}Th that
529 must be lost to explain the ^{232}Th data is 61%, 43%, 31% respectively. These values are up
530 to two times higher than the values calculated from the mass flux approach, but indicate that
531 loss of ^{230}Th during carbonate dissolution may be one of the processes responsible for the
532 apparent increase in ^{232}Th fluxes with depth.

533

534 The calculated deficit in ^{230}Th that is required to explain the observed trends in ^{230}Th -
535 normalised fluxes may be a result of advection, sediment redistribution or a combination of
536 all of the processes acting together, rather than only sediment dissolution. The size of the
537 ^{230}Th deficit must increase with depth in order to explain trends in ^{232}Th fluxes, so sediment
538 dissolution is a mechanism that could drive at least part of the trend, and is a process with a
539 well-defined depth dependence. In addition, if ^{230}Th is indeed lost from the sediment upon
540 carbonate dissolution and does not re-adsorb back to the sediment, there must exist some
541 mechanism which removes this ^{230}Th . Given previous observations in the Atlantic, lateral
542 advection of ^{230}Th seems a plausible mechanism (Moran et al., 2002; Marchal et al., 2007;
543 Hayes et al., 2015). A steady state scenario would require this laterally advected ^{230}Th to be
544 scavenged elsewhere, for example in areas with enhanced local scavenging such as
545 nepheloid layers or mid-ocean ridges (e.g. Hayes et al., 2015b).

546

547 5.4 The use of ^{230}Th -normalised ^{232}Th fluxes to estimate continental input

548 Despite the variation of apparent ^{232}Th fluxes with depth that we have identified, and the
549 uncertainties associated with such a variation, ^{230}Th -normalised ^{232}Th fluxes may still
550 represent a useful tool in determining continental fluxes to the sediment (Anderson et al.,
551 2016; Kienast et al., 2016). This is made clear when placed in the context of other

552 techniques that are available in order to estimate dust fluxes, such as models. These other
553 techniques can have uncertainties on the order of a factor of 10 (Mahowald et al., 2005) and
554 have not satisfactorily reproduced observational data for the modern day (Evan et al., 2014).
555 Calculated ^{232}Th fluxes for sediments at depths <1500 m are scattered and do not show a
556 recognisable trend with distance from the source of continental material (Figure 4c).
557 Therefore these samples cannot be considered to be accurately reproducing the trend of
558 modern dust input. Sediment samples at the greatest depths may have been subjected to
559 the greatest degree of the processes discussed above, such as carbonate dissolution. We
560 propose, therefore, that samples from the depth interval ~1500 -3000 m can give the best
561 estimate of representative ^{232}Th fluxes to the sediment in our study area (and therefore also
562 represent our best estimate of continental input), as summarised in Figure 6. Given the
563 processes affecting sedimentary $^{232}\text{Th}/^{230}\text{Th}$ from seasonal variations in the dust plume to
564 thorium advection, sediment redistribution and diagenesis, we would not expect a linear
565 trend of ^{232}Th fluxes from east to west. However, using this approach we do see an east to
566 west decrease in ^{232}Th flux of a factor of ~0.5. The average dissolved ^{232}Th flux
567 reconstructed from seawater reveals a similar change (a factor of ~0.7), although the
568 absolute ^{232}Th flux in the dissolved phase is approximately a factor of 4 lower (Figure 6).
569 This decrease in ^{232}Th flux is of the same order of magnitude to that presented by Anderson
570 et al., (2016) for a set of cores ~10° to the north (averaging a factor of ~0.8 decrease from
571 east to west when excluding data that lie closer to the continent than our samples). Data
572 from previous studies show good agreement with the range of ^{232}Th fluxes calculated in this
573 study at SLR and the central tropical Atlantic (Figure 6; Francois and Bacon, 1991; core
574 VM20-234, Williams et al., 2016). The longitudinal transect of sedimentary ^{232}Th fluxes
575 presented by Anderson et al. (2016) are on average ~32% higher in the East and ~46%
576 lower values in the West than the 1500-3000 m fluxes of our transect. Differences in the
577 latitude of the transects may contribute to some of the disparity. At CR the values of ^{232}Th
578 flux are considerably elevated above those found at a similar longitude from this study
579 (Vema site), likely as a result of lithogenic sediment input to CR from the Amazon River
580 (Francois and Bacon, 1991; Figure 6).

581

582 5.5 Apparent fractional solubility of ^{232}Th

583 Estimates of ^{232}Th solubility represent a large uncertainty in calculating detrital fluxes from
584 seawater $^{232}\text{Th}/^{230}\text{Th}$ ratios (Hsieh et al., 2011; Anderson et al., 2016). Estimates of this
585 solubility may also be important in relation to the release of other trace metals from detrital
586 material in seawater (Hayes et al., 2015c; Anderson et al., 2016). Our seawater $^{232}\text{Th}/^{230}\text{Th}$
587 ratios paired with sedimentary ratios from the nearest sample sites can be used to derive an
588 apparent fractional solubility of ^{232}Th from dust, with the caveat that if not all dissolved ^{232}Th

589 is derived from the dissolution of dust added at the surface, then the solubility will be
590 overestimated by a degree that is dependent on the amount of advected ^{232}Th (Figure 7).

591

592 This estimation can be made because the difference between the seawater $^{232}\text{Th}/^{230}\text{Th}$ ratio
593 and the sedimentary ratio is only a function of how much ^{232}Th is released from the dust to
594 the water, i.e. if half of the ^{232}Th were released, the seawater and sediment $^{232}\text{Th}/^{230}\text{Th}$ ratio
595 would differ by a factor of two (Equation 4).

596

597 Equation 4: Apparent fractional solubility = $[\text{}^{232}\text{Th}/\text{}^{230}\text{Th}]_{\text{SW}} / [\text{}^{232}\text{Th}/\text{}^{230}\text{Th}]_{\text{Sed}}$

598

599 Our results indicate that the apparent fractional solubility of ^{232}Th from continental material is
600 not systematically dependent on depth at any of the sample locations (Figure 7). The
601 calculated solubilities range from 18 to 67 %, with an average solubility of 33%. Of the
602 solubilities calculated, 14 out of 17 values lie in the relatively narrow range 18-35% (Figure
603 7; supplementary information). These estimates are generally consistent with some of the
604 upper estimates of ^{232}Th solubility made by previous studies. Hayes et al., (2013) make
605 model-based estimates of ^{232}Th solubility up to 40%, although they prefer an estimate closer
606 to 20% based on the refractory nature of Th. Okubo et al., (2013) measure the solubility of
607 ^{232}Th from atmospherically deposited aerosol samples to be ~20% and Arraes-Mescoff et al.,
608 (2001) measure the percentage dissolution of ^{232}Th from particles to be up to ~13%. A
609 recent study from the North Atlantic estimates the likely range of thorium solubilities at
610 depths of 100 m to lie between 14-28% (Hayes et al., 2017), a range that agrees with the
611 majority of our estimates (Figure 7). The authors also calculate higher solubilities between
612 31-63% at depths up to 500 m, but conclude that these estimates may be influenced by
613 water masses bearing a ^{232}Th signature carried from elsewhere. These higher estimates still
614 lie within the solubility range estimated in this study.

615

616 It is possible that because seawater samples were collected close to the ocean floor that the
617 dissolution of any re-suspended sediments could lead to elevated ^{232}Th concentrations in the
618 seawater samples, and therefore bias the estimate of solubility, however the relatively
619 narrow range of solubilities from various locations and depths would argue against this
620 process being dominant. It is also possible, given the relatively large core-top ages of some
621 of our sediments, that the seawater-sediment comparison results in comparison of thorium
622 signals with different ages, and so the estimates of solubility could be dependent on changes
623 in ^{232}Th fluxes with time.

624

625 The average value of apparent solubility from this study of $29 \pm 3\%$ (2 s.e., $n=15$, excluding
626 the two outliers circled in Figure 7), could be used as a general estimate of ^{232}Th solubility for
627 studies that require such a value to extrapolate total ^{232}Th fluxes and detrital fluxes from
628 dissolved ^{232}Th fluxes (e.g. Hsieh et al., 2011; Hayes et al., 2013; Deng et al., 2014). This
629 value is slightly higher than the range suggested by Hayes et al. (2013) of $20 \pm 5\%$, and may
630 be more appropriate as our study utilizes co-located samples to estimate solubility
631 (Anderson et al., 2016).

632

633 6. Conclusions

634 Both seawater and sedimentary $^{232}\text{Th}/^{230}\text{Th}$ ratios show a broad decreasing trend moving
635 west away from the African continent towards South America, consistent with expected
636 overall dust deposition patterns in the Tropical North Atlantic. However, the large depth
637 dependence of sedimentary ^{232}Th fluxes observed at all five of our sample locations
638 suggests an additional degree of complexity associated with the interpretation of ^{230}Th -
639 normalised ^{232}Th fluxes.

640

641 The mechanism that leads to increased ^{232}Th fluxes at depth remains uncertain, and may be
642 due to geochemical processes (such as the loss of ^{230}Th upon carbonate dissolution),
643 physical processes (e.g. advection by deep waters or sediment redistribution), or a
644 combination of processes. Further study of ^{232}Th fluxes with depth in seawater, particles and
645 sediment phases at other locations are required to further investigate these mechanisms.
646 The combined use of other geochemical proxies for lithogenic inputs which may not be
647 sensitive to the processes described above (such as $^4\text{He}/^3\text{He}$) may help to disentangle some
648 of the possible mechanisms acting. Notwithstanding this depth dependence, we propose that
649 ^{232}Th fluxes measured in sediment in the depth interval between ~ 1500 -3000 m provide the
650 best estimate of representative ^{232}Th fluxes at our sample sites. By combining
651 measurements of $^{232}\text{Th}/^{230}\text{Th}$ in seawater and core-top sediments we have been able to
652 derive an apparent fractional solubility of ^{232}Th of $29 \pm 3\%$, in reasonable agreement with the
653 upper end of existing estimates.

654

655 Acknowledgements

656 We acknowledge the science team and crew of JC094 for collecting and supplying sample
657 material. The authors would like to thank Carolyn Taylor for her laboratory assistance in
658 performing sediment leaching experiments and Chris Coath for his help in the Bristol Isotope
659 Group. We acknowledge funding from The European Research Council, a Marie Curie
660 Reintegration grant, the Leverhulme Trust and a Natural Environment Research Council
661 studentship.

662
663
664
665
666
667
668
669
670
671
672
673
674
675
676
677

678 **References**

- 679 Anderson R. F., Cheng H., Edwards R. L., Fleisher M. Q., Hayes C. T., Huang K.-F., Kadko
680 D., Lam P. J., Landing W. M., Lao Y., Lu Y., Measures C. I., Moran S. B., Morton P.
681 L., Ohnemus D. C., Robinson L. F. and Shelley R. U. (2016) How well can we quantify
682 dust deposition to the ocean? *Philos. Trans. R. Soc. A Math. Phys. Eng. Sci.* 374.
- 683 Anderson R. F., Bacon M. P. and Brewer P. G. (1983) Removal of ²³⁰Th and ²³¹Pa at ocean
684 margins. *Earth Planet. Sci. Lett.* **66**, 73–90..
- 685 Anderson R. F., Fleisher M. Q. and Lao Y. (2006) Glacial-interglacial variability in the
686 delivery of dust to the central equatorial Pacific Ocean. *Earth Planet. Sci. Lett.* **242**,
687 406–414.
- 688 Arraes-Mescoff R., Roy-Barman M., Coppola L., Souhaut M., Tachikawa K., Jeandel C.,
689 Sempéré R. and Yoro C. (2001) The behavior of Al, Mn, Ba, Sr, REE and Th isotopes
690 during in vitro degradation of large marine particles. *Mar. Chem.* **73**, 1–19.
- 691 Auro M. E., Robinson L. F., Burke A., Bradtmiller L. I., Fleisher M. Q. and Anderson R. F.
692 (2012) Improvements to ²³²-thorium, ²³⁰-thorium, and ²³¹-protactinium analysis in
693 seawater arising from GEOTRACES intercalibration. *Limnol. Oceanogr. Methods* **10**,
694 464–474.
- 695 Bacon M. P. and Anderson R. F. (1982) Distribution of thorium isotopes between dissolved
696 and particulate forms in the deep sea. *J. Geophys. Res.* **87**, 2045.
- 697 Beaulieu S. E., Baker E. T. and German C. R. (2015) Where are the undiscovered
698 hydrothermal vents on oceanic spreading ridges? *Deep Sea Res. Part II Top. Stud.*
699 *Oceanogr.* 121, 202–212.
- 700 Broecker W. S., Kaufman A. and Trier R. M. (1973) The residence time of thorium in surface
701 sea water and its implications regarding the rate of reactive pollutants. *Earth Planet. Sci.*
702 *Lett.* **20**, 35–44.
- 703 Cakmur R. V., Miller R. L., Perlwitz J., Geogdzhayev I. V., Ginoux P., Koch D., Kohfeld K.
704 E., Tegen I. and Zender C. S. (2006) Constraining the magnitude of the global dust cycle
705 by minimizing the difference between a model and observations. *J. Geophys. Res.*
706 *Atmos.* **111**.
- 707 Castillo S., Moreno T., Querol X., Alastuey A., Cuevas E., Herrmann L., Mounkaila M. and
708 Gibbons W. (2008) Trace element variation in size-fractionated African desert dusts. *J.*
709 *Arid Environ.* **72**, 1034–1045.
- 710 Costa K. and McManus J. (2017) Efficacy of ²³⁰Th normalization in sediments from the
711 Juan de Fuca Ridge, northeast Pacific Ocean. *Geochim. Cosmochim. Acta* **197**, 215–225.
- 712 Chen T., Robinson L. F., Burke A., Southon J., Spooner P., Morris P. J. and Ng H. C. (2015)
713 Synchronous centennial abrupt events in the ocean and atmosphere during the last
714 deglaciation. *Sci.* 349, 1537–1541.
- 715 Cheng H., Edwards R. L., Shen C.-C., Polyak V. J., Asmerom Y., Woodhead J., Hellstrom J.,
716 Wang Y., Kong X., Spötl C., Wang X. and Jr. E. C. A. (2013) Improvements in ²³⁰Th
717 dating, ²³⁰Th and ²³⁴U half-life values, and U–Th isotopic measurements by multi-
718 collector inductively coupled plasma mass spectrometry. *Earth Planet. Sci. Lett.* **371–**
719 **372**, 82–91.
- 720 Costa K. M., McManus J. F., Anderson R. F., Ren H., Sigman D. M., Winckler G., Fleisher
721 M. Q., Marcantonio F. and Ravelo A. C. (2016) No iron fertilization in the equatorial
722 Pacific Ocean during the last ice age. *Nature* **529**, 519–522.
- 723 De Villiers S. (2005) Foraminiferal shell-weight evidence for sedimentary calcite dissolution
724 above the lysocline. *Deep. Res. Part I Oceanogr. Res. Pap.* **52**, 671–680.
- 725 Deng F., Thomas A. L., Rijkenberg M. J. A. and Henderson G. M. (2014) Controls on
726 seawater ²³¹Pa, ²³⁰Th and ²³²Th concentrations along the flow paths of deep waters in
727 the Southwest Atlantic. *Earth Planet. Sci. Lett.* **390**, 93–102.

728 Eglinton T. I., Eglinton G., Dupont L., Sholkovitz E. R., Montluçon D. and Reddy C. M.
729 (2002) Composition, age, and provenance of organic matter in NW African dust over the
730 Atlantic Ocean. *Geochemistry, Geophys. Geosystems* **3**, 1–27.

731 Evan A. T., Flamant C., Fiedler S. and Doherty O. (2014) An analysis of aeolian dust in
732 climate models. *Geophys. Res. Lett.* **41**, 5996–6001.

733 Francois R. and Bacon M. P. (1991) Variations in Terrigenous Input Into the Deep Equatorial
734 Atlantic During the Past 24,000 Years. *Science* **251**, 1473–1476.

735 Francois R., Bacon M. P. and Suman D. O. (1990) Thorium 230 profiling in deep-sea
736 sediments: High-resolution records of flux and dissolution of carbonate in the equatorial
737 Atlantic during the last 24,000 years. *Paleoceanography* **5**, 761–787.

738 Francois R., Frank M., van der Loeff M. M. and Bacon M. P. (2004) 230Th normalization:
739 An essential tool for interpreting sedimentary fluxes during the late Quaternary.
740 *Paleoceanography* **19**.

741 Goudie A. S. and Middleton N. J. (2001) Saharan dust storms: nature and consequences.
742 *Earth-Science Rev.* **56**, 179–204.

743 Harrison S. P., Kohfeld K. E., Roelandt C. and Claquin T. (2001) The role of dust in climate
744 changes today, at the last glacial maximum and in the future. *Earth-Science Rev.* **54**, 43–
745 80.

746 Hayes C. T., Anderson R. F., Fleisher M. Q., Huang K.-F., Robinson L. F., Lu Y., Cheng H.,
747 Edwards R. L. and Moran S. B. (2015a) 230 Th and 231 Pa on GEOTRACES GA03, the
748 US GEOTRACES North Atlantic transect, and implications for modern and
749 paleoceanographic chemical fluxes. *Deep Sea Res. Part II Top. Stud. Oceanogr.* **116**,
750 29–41.

751 Hayes C. T., Anderson R. F., Fleisher M. Q., Serno S., Winckler G. and Gersonde R. (2013)
752 Quantifying lithogenic inputs to the North Pacific Ocean using the long-lived thorium
753 isotopes. *Earth Planet. Sci. Lett.* **383**, 16–25.

754 Hayes C. T., Anderson R. F., Fleisher M. Q., Vivancos S. M., Lam P. J., Ohnemus D. C.,
755 Huang K.-F., Robinson L. F., Lu Y., Cheng H., Edwards R. L. and Moran S. B. (2015b)
756 Intensity of Th and Pa scavenging partitioned by particle chemistry in the North Atlantic
757 Ocean. *Mar. Chem.* **170**, 49–60.

758 Hayes C. T., Fitzsimmons J. N., Boyle E. A., McGee D., Anderson R. F., Weisend R. and
759 Morton P. L. (2015c) Thorium isotopes tracing the iron cycle at the Hawaii Ocean Time-
760 series Station ALOHA. *Geochim. Cosmochim. Acta* **169**, 1–16.

761 Hayes C. T., Rosen J., McGee D. and Boyle E. A. (2017) Thorium distributions in high and
762 low dust regions and the significance for iron supply. *Global Biogeochem. Cycles*.

763 Henderson G. M. and Anderson R. F. (2003) The U-series Toolbox for Paleoceanography.
764 *Rev. Mineral. Geochemistry* **52**, 493–531.

765 Henderson G. M., Heinze C., Anderson R. F. and Winguth A. M. E. (1999) Global
766 distribution of the 230Th flux to ocean sediments constrained by GCM modelling. *Deep*
767 *Sea Res. Part I Oceanogr. Res. Pap.* **46**, 1861–1893

768 Hoffmann D. L., Prytulak J., Richards D. A., Elliott T., Coath C. D., Smart P. L. and Scholz
769 D. (2007) Procedures for accurate U and Th isotope measurements by high precision
770 MC-ICPMS. *Int. J. Mass Spectrom.* **264**, 97–109.

771 Holden N. E. (1990) Total half-lives for selected nuclides. *Pure Appl. Chem.* **62**, 941–958.

772 Hsieh Y. Te, Henderson G. M. and Thomas A. L. (2011) Combining seawater 232Th and
773 230Th concentrations to determine dust fluxes to the surface ocean. *Earth Planet. Sci.*
774 *Lett.* **312**, 280–290.

775 Hydes D. J. (1983) Distribution of aluminium in waters of the North East Atlantic 25°N to
776 35°N. *Geochim. Cosmochim. Acta* **47**, 967–973.

- 777 Jacobel A. W., McManus J. F., Anderson R. F. and Winckler G. (2016) Large deglacial shifts
778 of the Pacific Intertropical Convergence Zone. *Nat Commun* **7**.
- 779 Jickells T. D., An Z. S., Andersen K. K., Baker A. R., Bergametti G., Brooks N., Cao J. J.,
780 Boyd P. W., Duce R. A., Hunter K. A., Kawahata H., Kubilay N., laRoche J., Liss P. S.,
781 Mahowald N., Prospero J. M., Ridgwell A. J., Tegen I. and Torres R. (2005) Global Iron
782 Connections Between Desert Dust, Ocean Biogeochemistry, and Climate. *Sci.* **308**, 67–
783 71.
- 784 Kienast S. S., Winckler G., Lippold J., Albani S. and Mahowald N. M. (2016) Tracing dust
785 input to the global ocean using thorium isotopes in marine sediments: ThoroMap. *Global*
786 *Biogeochem. Cycles* **30**, 1526–1541.
- 787 Kohfeld K. E. and Harrison S. P. (2001) DIRTMAP: the geological record of dust. *Earth-*
788 *Science Rev.* **54**, 81–114.
- 789 Kretschmer S., Geibert W., van der Loeff M. M. R. and Mollenhauer G. (2010) Grain size
790 effects on ²³⁰Thxs inventories in opal-rich and carbonate-rich marine sediments. *Earth*
791 *Planet. Sci. Lett.* **294**, 131–142.
- 792 Lawrence C. R. and Neff J. C. (2009) The contemporary physical and chemical flux of
793 aeolian dust: A synthesis of direct measurements of dust deposition. *Chem. Geol.* **267**,
794 46–63.
- 795 Lam P. J., Ohnemus D. C. and Auro M. E. (2015) Size-fractionated major particle
796 composition and concentrations from the US GEOTRACES north Atlantic zonal
797 transect. *Deep Sea Res. Part II Top. Stud. Oceanogr.* **116**, 303–320.
- 798 Lam P. J., Robinson L. F., Blusztajn J., Li C., Cook M. S., McManus J. F. and Keigwin L. D.
799 (2013) Transient stratification as the cause of the North Pacific productivity spike during
800 deglaciation. *Nat. Geosci* **6**, 622–626.
- 801 Lerner P., Marchal O., Lam P. J., Anderson R. F., Buesseler K., Charette M. A., Edwards R.
802 L., Hayes C. T., Huang K.-F., Lu Y., Robinson L. F. and Solow A. (2016) Testing
803 models of thorium and particle cycling in the ocean using data from station GT11-22 of
804 the U.S. GEOTRACES North Atlantic section. *Deep Sea Res. Part I Oceanogr. Res.*
805 *Pap.* **113**, 57–79.
- 806 Lopez G. I., Marcantonio F., Lyle M. and Lynch-Stieglitz J. (2015) Dissolved and particulate
807 ²³⁰Th–²³²Th in the Central Equatorial Pacific Ocean: Evidence for far-field transport
808 of the East Pacific Rise hydrothermal plume. *Earth Planet. Sci. Lett.* **431**, 87–95.
- 809 Maher B. A., Prospero J. M., Mackie D., Gaiero D., Hesse P. P. and Balkanski Y. (2010)
810 Global connections between aeolian dust, climate and ocean biogeochemistry at the
811 present day and at the last glacial maximum. *Earth-Science Rev.* **99**, 61–97.
- 812 Mahowald N. M., Baker A. R., Bergametti G., Brooks N., Duce R. A., Jickells T. D., Kubilay
813 N., Prospero J. M. and Tegen I. (2005) Atmospheric global dust cycle and iron inputs to
814 the ocean. *Global Biogeochem. Cycles* **19**.
- 815 Marcantonio F., Lyle M. and Ibrahim R. (2014) Particle sorting during sediment
816 redistribution processes and the effect on ²³⁰Th-normalized mass accumulation rates.
817 *Geophys. Res. Lett.* **41**, 5547–5554.
- 818 Marchal O., François R. and Scholten J. (2007) Contribution of ²³⁰Th measurements to the
819 estimation of the abyssal circulation. *Deep Sea Res. Part I Oceanogr. Res. Pap.* **54**, 557–
820 585.
- 821 McCave I. N. (1986) Local and global aspects of the bottom nepheloid layers in the world
822 ocean. *Netherlands J. Sea Res.* **20**, 167–181.
- 823 McGee D., deMenocal P. B., Winckler G., Stuut J. B. W. and Bradtmiller L. I. (2013) The
824 magnitude, timing and abruptness of changes in North African dust deposition over the
825 last 20,000 yr. *Earth Planet. Sci. Lett.* 371–372, 163–176

- 826 McGee D., Marcantonio F. and Lynch-Stieglitz J. (2007) Deglacial changes in dust flux in
827 the eastern equatorial Pacific. *Earth Planet. Sci. Lett.* **257**, 215–230.
- 828 McGee D., Marcantonio F., McManus J. F. and Winckler G. (2010) The response of excess
829 ^{230}Th and extraterrestrial ^3He to sediment redistribution at the Blake Ridge, western
830 North Atlantic. *Earth Planet. Sci. Lett.* **299**, 138–149.
- 831 McGee D., Winckler G., Borunda A., Serno S., Anderson R. F., Recasens C., Bory A.,
832 Gaiero D., Jaccard S. L., Kaplan M., McManus J. F., Revel M. and Sun Y. (2016)
833 Tracking eolian dust with helium and thorium: Impacts of grain size and provenance.
834 *Geochim. Cosmochim. Acta* **175**.
- 835 Measures C. I., Landing W. M., Brown M. T. and Buck C. S. (2008) High-resolution Al and
836 Fe data from the Atlantic Ocean CLIVAR-CO2 Repeat Hydrography A16N transect:
837 Extensive linkages between atmospheric dust and upper ocean geochemistry. *Global*
838 *Biogeochem. Cycles* **22**.
- 839 Moran S. B., Shen C. C., Edmonds H. N., Weinstein S. E., Smith J. N. and Edwards R. L.
840 (2002) Dissolved and particulate ^{231}Pa and ^{230}Th in the Atlantic Ocean: Constraints on
841 intermediate/deep water age, boundary scavenging, and $^{231}\text{Pa}/^{230}\text{Th}$ fractionation.
842 *Earth Planet. Sci. Lett.* **203**, 999–1014.
- 843 Mortlock R. A. and Froelich P. N. (1989) A simple method for the rapid determination of
844 biogenic opal in pelagic marine sediments. *Deep Sea Res. Part A. Oceanogr. Res. Pap.*
845 **36**, 1415–1426.
- 846 Niedermeier N., Held A., Müller T., Heinold B., Schepanski K., Tegen I., Kandler K., Ebert
847 M., Weinbruch S., Read K., Lee J., Fomba K. W., Müller K., Herrmann H. and
848 Wiedensohler A. (2014) Mass deposition fluxes of Saharan mineral dust to the tropical
849 northeast Atlantic Ocean: an intercomparison of methods. *Atmos. Chem. Phys.* **14**,
850 2245–2266.
- 851 Okubo A., Obata H., Gamo T. and Yamada M. (2012) ^{230}Th and ^{232}Th distributions in mid-
852 latitudes of the North Pacific Ocean: Effect of bottom scavenging. *Earth Planet. Sci.*
853 *Lett.* **339–340**, 139–150.
- 854 Peine F., Turnewitsch R., Mohn C., Reichelt T., Springer B. and Kaufmann M. (2009) The
855 importance of tides for sediment dynamics in the deep sea—evidence from the
856 particulate-matter tracer ^{234}Th in deep-sea environments with different tidal forcing.
857 *Deep Sea Res. Part I Oceanogr. Res. Pap.* **56**, 1182–1202.
- 858 Pourmand A., Marcantonio F. and Schulz H. (2004) Variations in productivity and eolian
859 fluxes in the northeastern Arabian Sea during the past 110 ka. *Earth Planet. Sci. Lett.*
860 **221**, 39–54.
- 861 Ratmeyer V., Fischer G. and Wefer G. (1999) Lithogenic particle fluxes and grain size
862 distributions in the deep ocean off northwest Africa: Implications for seasonal changes
863 of aeolian dust input and downward transport. *Deep Sea Res. Part I Oceanogr. Res. Pap.*
864 **46**, 1289–1337.
- 865 Ridley D. A., Heald C. L. and Ford B. (2012) North African dust export
866 and deposition: A satellite and model perspective. *J. Geophys. Res. Atmos.* **117**.
- 866 Robinson L. F. (2014) RRS James Cook Cruise JC094, October 13–November 30 2013,
867 Tenerife-Trinidad. TROPICS, Tracing Oceanic Processes using Corals and Sediments.
868 Reconstructing abrupt Changes in Chemistry and Circulation of the Equatorial Atlantic
869 Ocean. Available at: <http://epic.awi.de/35605/>
- 870 Robinson L. F., Belshaw N. S. and Henderson G. M. (2004) U and Th concentrations and
871 isotope ratios in modern carbonates and waters from the Bahamas. *Geochim.*
872 *Cosmochim. Acta* **68**, 1777–1789.
- 873 Robinson L. F., Noble T. L. and McManus J. F. (2008) Measurement of adsorbed and total
874 $^{232}\text{Th}/^{230}\text{Th}$ ratios from marine sediments. *Chem. Geol.* **252**, 169–179.

875 Roy-Barman M. (2009) Modelling the effect of boundary scavenging on Thorium and
876 Protactinium profiles in the ocean. *Biogeosciences* **6**, 3091–3107.

877 Serno S., Winckler G., Anderson R. F., Hayes C. T., McGee D., Machalett B., Ren H., Straub
878 S. M., Gersonde R. and Haug G. H. (2014) Eolian dust input to the Subarctic North
879 Pacific. *Earth Planet. Sci. Lett.* **387**, 252–263.

880 Singh A. K., Marcantonio F. and Lyle M. (2013) Water column ²³⁰Th systematics in the
881 eastern equatorial Pacific Ocean and implications for sediment focusing. *Earth Planet.*
882 *Sci. Lett.* **362**, 294–304.

883 Stanley D. J. and Taylor P. T. (1977) Sediment transport down a seamount flank by a
884 combined current and gravity process. *Mar. Geol.* **23**, 77–88.

885 Taylor S. R. and McLennan S. . (1985) The continental crust: Its composition and evolution.
886 *McClelland, Blackwell Sci. Publ.* **21**, 85–86.

887 Thomson J., Colley S., Anderson R., Cook G. T., MacKenzie A. B. and Harkness D. D.
888 (1993) Holocene sediment fluxes in the northeast Atlantic from ²³⁰Th excess and
889 radiocarbon measurements. *Paleoceanography* **8**, 631–650.

890 Thomson J., Green D. R. H., van Calsteren P., Richter T. O. and van Weering T. C. E. (2006)
891 Holocene sediment deposition on a NE Atlantic transect including Feni Drift quantified
892 by radiocarbon and ²³⁰Th excess methods. *Earth Planet. Sci. Lett.* **242**, 170–185.

893 Thomson J., Nixon S., Summerhayes C. P., Schönfeld J., Zahn R. and Grootes P. (1999)
894 Implications for sedimentation changes on the Iberian margin over the last two
895 glacial/interglacial transitions from (²³⁰Th excess)₀ systematics. *Earth Planet. Sci. Lett.*
896 **165**, 255–270.

897 Wang X., Murtugudde R., Hackert E. and Marañón E. (2013) Phytoplankton carbon and
898 chlorophyll distributions in the equatorial Pacific and Atlantic: a basin-scale
899 comparative study. *J. Mar. Syst.* **109**, 138–148.

900 Williams R. H., McGee D., Kinsley C. W., Ridley D. A., Hu S., Fedorov A., Tal I., Murray
901 R. W. and deMenocal P. B. (2016) Glacial to Holocene changes in trans-Atlantic
902 Saharan dust transport and dust-climate feedbacks. *Sci. Adv.* **2**.

903 Winckler G., Anderson R. F., Fleisher M. Q., McGee D. and Mahowald N. (2008) Covariant
904 glacial-interglacial dust fluxes in the equatorial Pacific and Antarctica. *Science* **320**, 93–
905 96.

906
907
908
909
910
911
912
913

Figure1

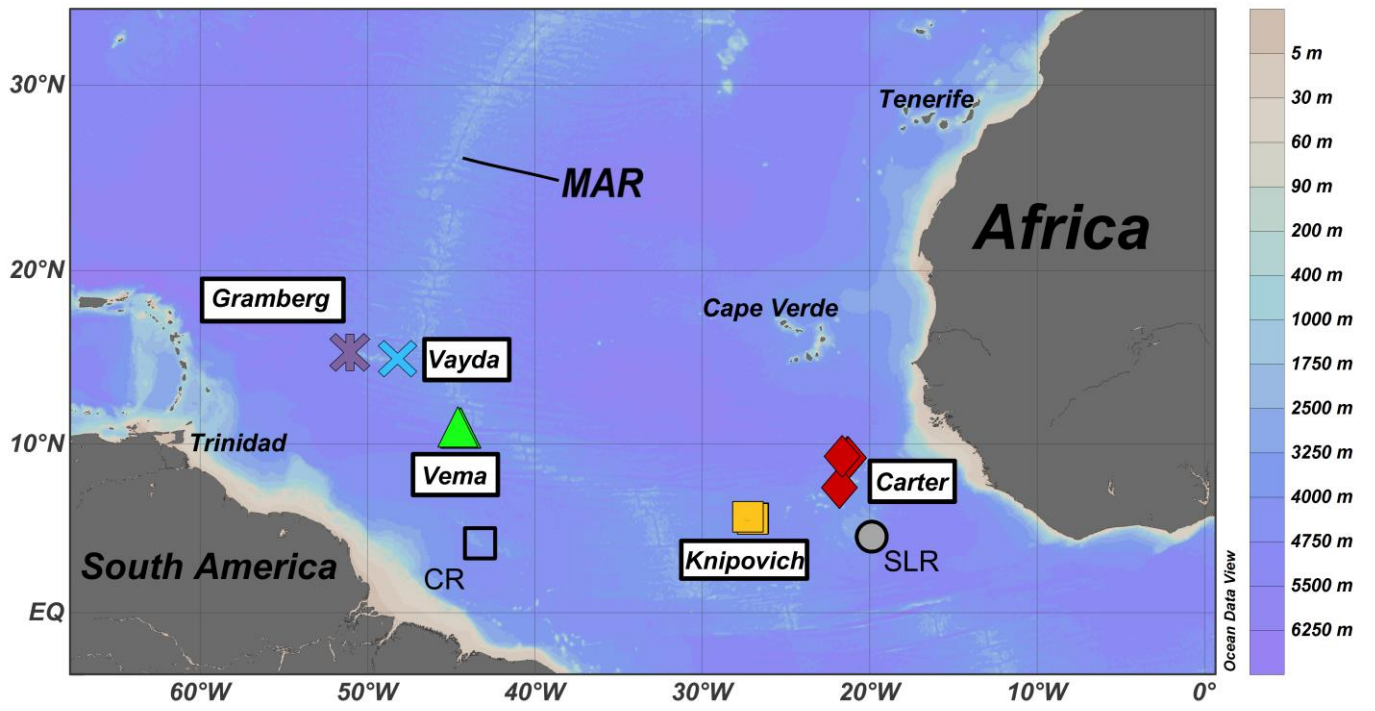


Figure 1. Map of JC094 sites where the samples of sediment and seawater for this study were collected. The sites are named based on their proximity to bathymetric features. The start and end points of the cruise are indicated (Tenerife and Trinidad respectively) as well as the Mid-Atlantic ridge (MAR). CR = Ceara rise, SLR= Sierra Leone rise (Francois et al., 1990).

Figure2

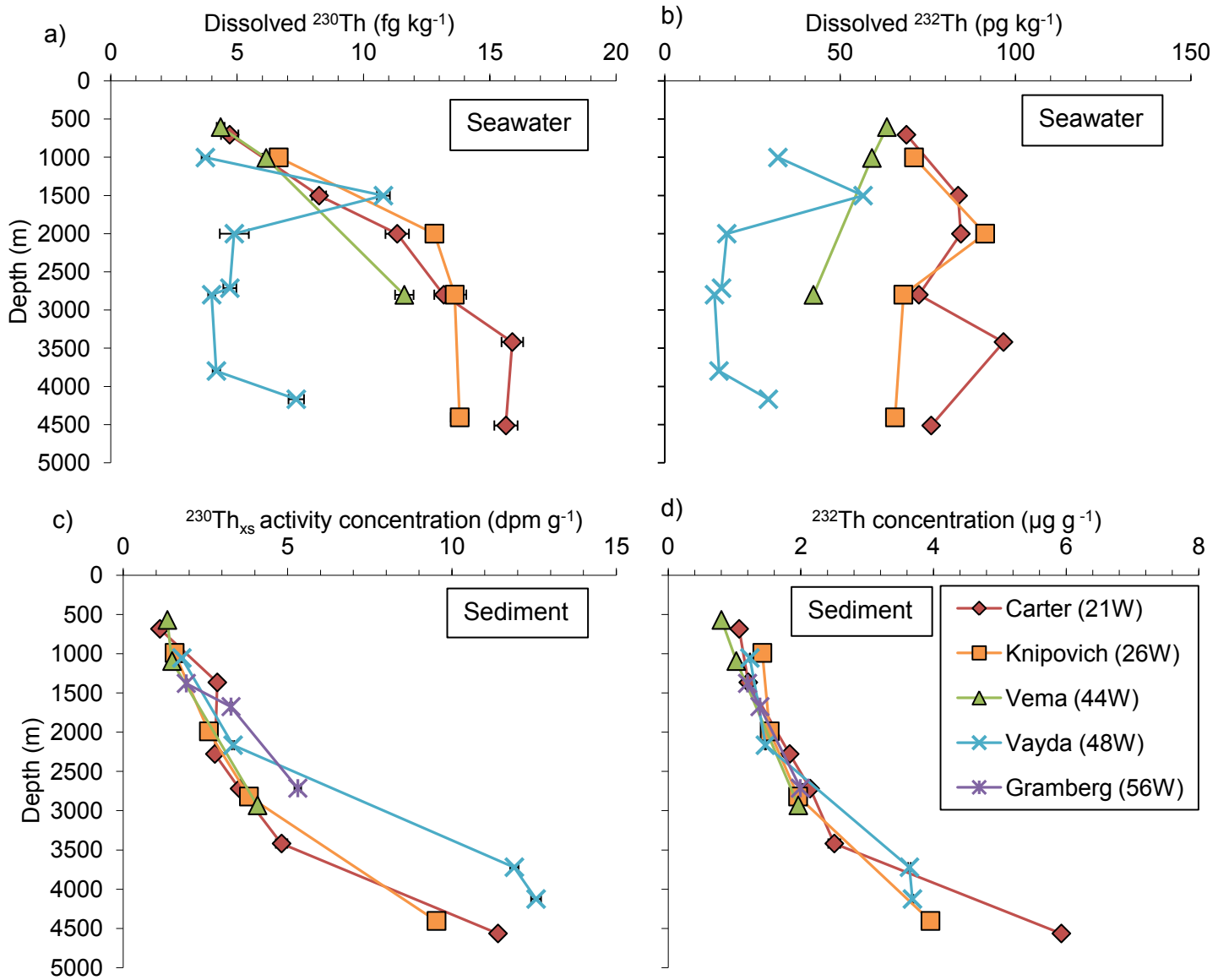


Figure 2. Concentrations of a) ^{230}Th and b) ^{232}Th in filtered seawater samples and concentrations of c) $^{230}\text{Th}_{\text{xs}}$ and d) ^{232}Th in sediment core-tops. Where error bars are not visible they are smaller than the symbols used. The approximate longitude of each sampling locations is given in the key.

Figure3

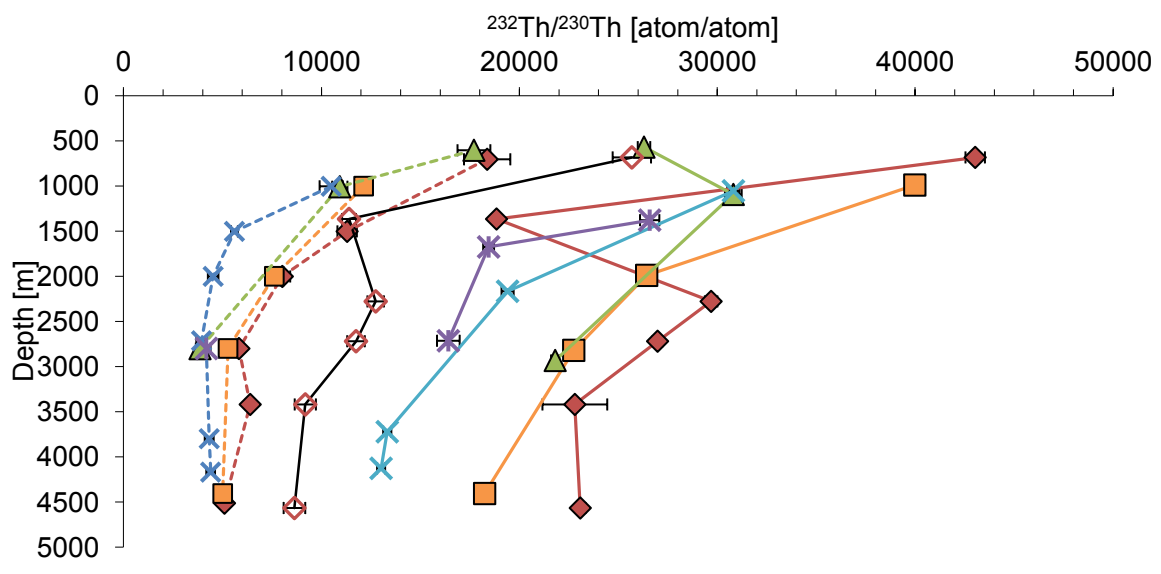


Figure 3. Atomic ratios of $^{232}\text{Th}/^{230}\text{Th}_{\text{xs}}$ in seawater (dashed lines) and core-top sediment samples (solid lines) with depth. Ratios derived from leaching of Carter sediments are presented as hollow diamonds. Error bars represent 2 standard deviations from the mean, reflecting analytical uncertainty.

Figure 4

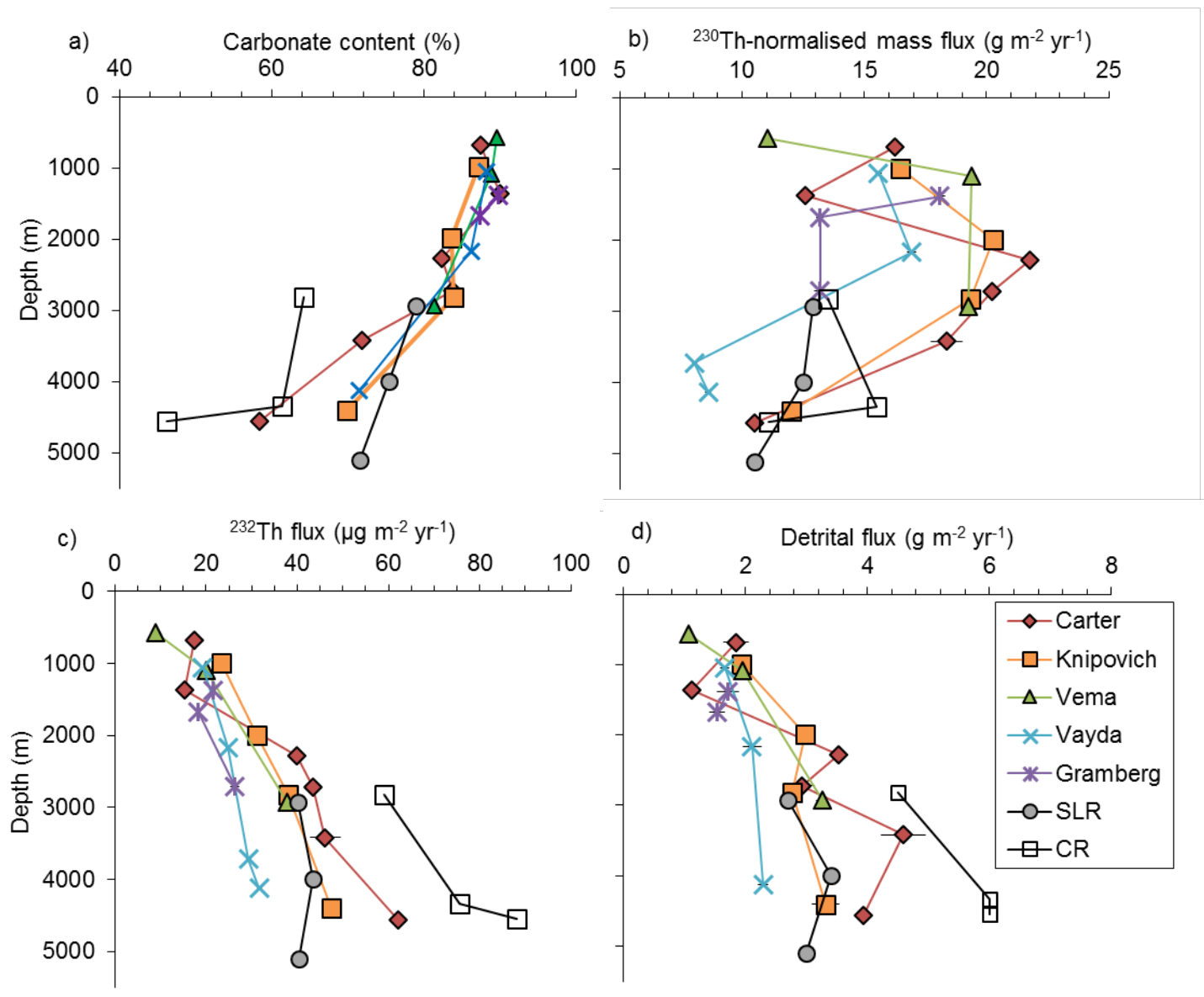


Figure 4. a) Carbonate content, b) ^{230}Th -normalised mass fluxes c) ^{230}Th -normalised ^{232}Th fluxes d) ^{230}Th -normalised detrital fluxes. Error bars give 2 standard deviations from the mean, and represent the analytical uncertainty. SLR (= Sierra Leone rise) and CR (= Ceara rise) are data from Francois et al. (1990), from samples at the shallowest possible core depths (<3.5 cm from the core-top) all with model ages of <2 kyr (Francois et al., 1990).

Figure5 revised

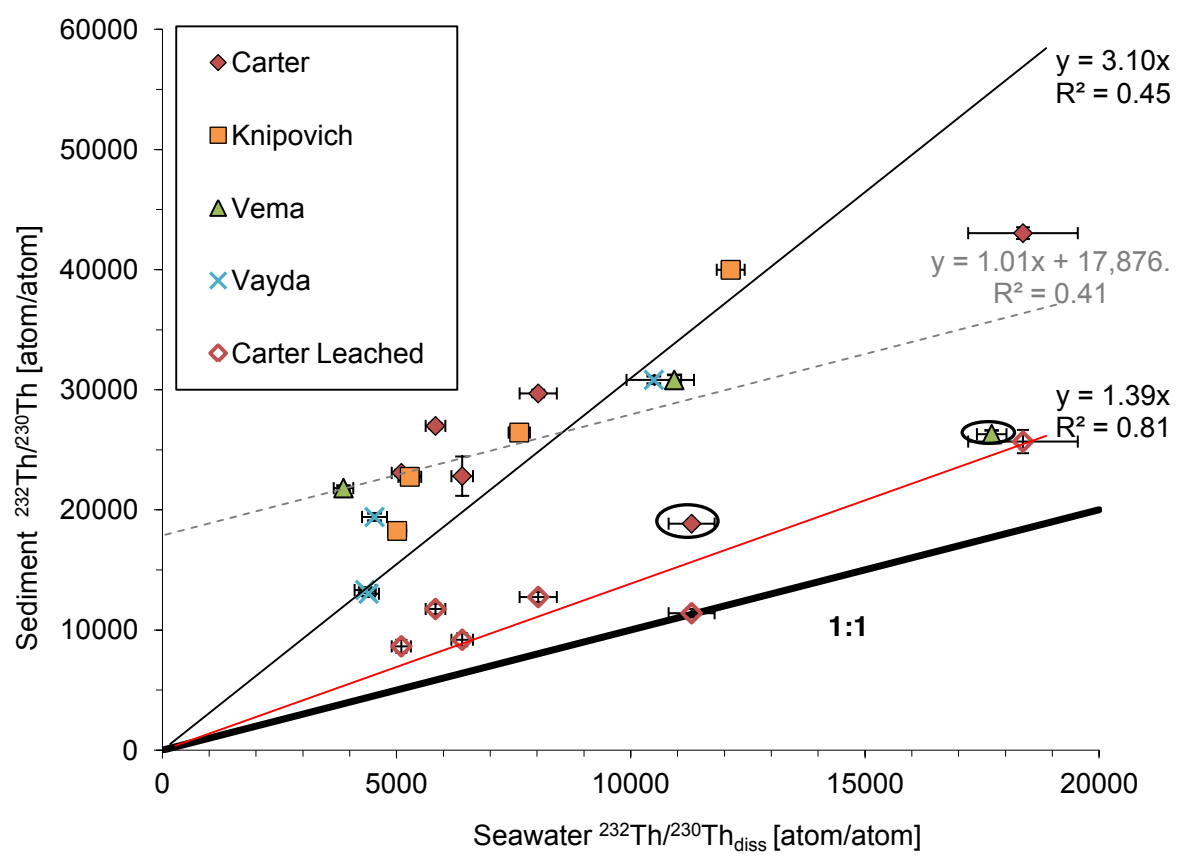


Figure 5. Comparison of $^{232}\text{Th}/^{230}\text{Th}_{\text{xs}}$ in sediment core-tops and seawater samples (solid symbols). A linear regression for sediment and seawater data is shown by the thin black line, with the two circled data points not included in the regression (inclusion of these data gives $R^2 = 0.41$, shown by the grey dashed regression line). Hollow red diamonds indicate leached core-top sediments and seawater $^{232}\text{Th}/^{230}\text{Th}$ from Carter Seamount; a linear regression is shown by the red line. All error bars represent 2 standard deviations from the mean, reflecting the analytical uncertainty.

Figure6

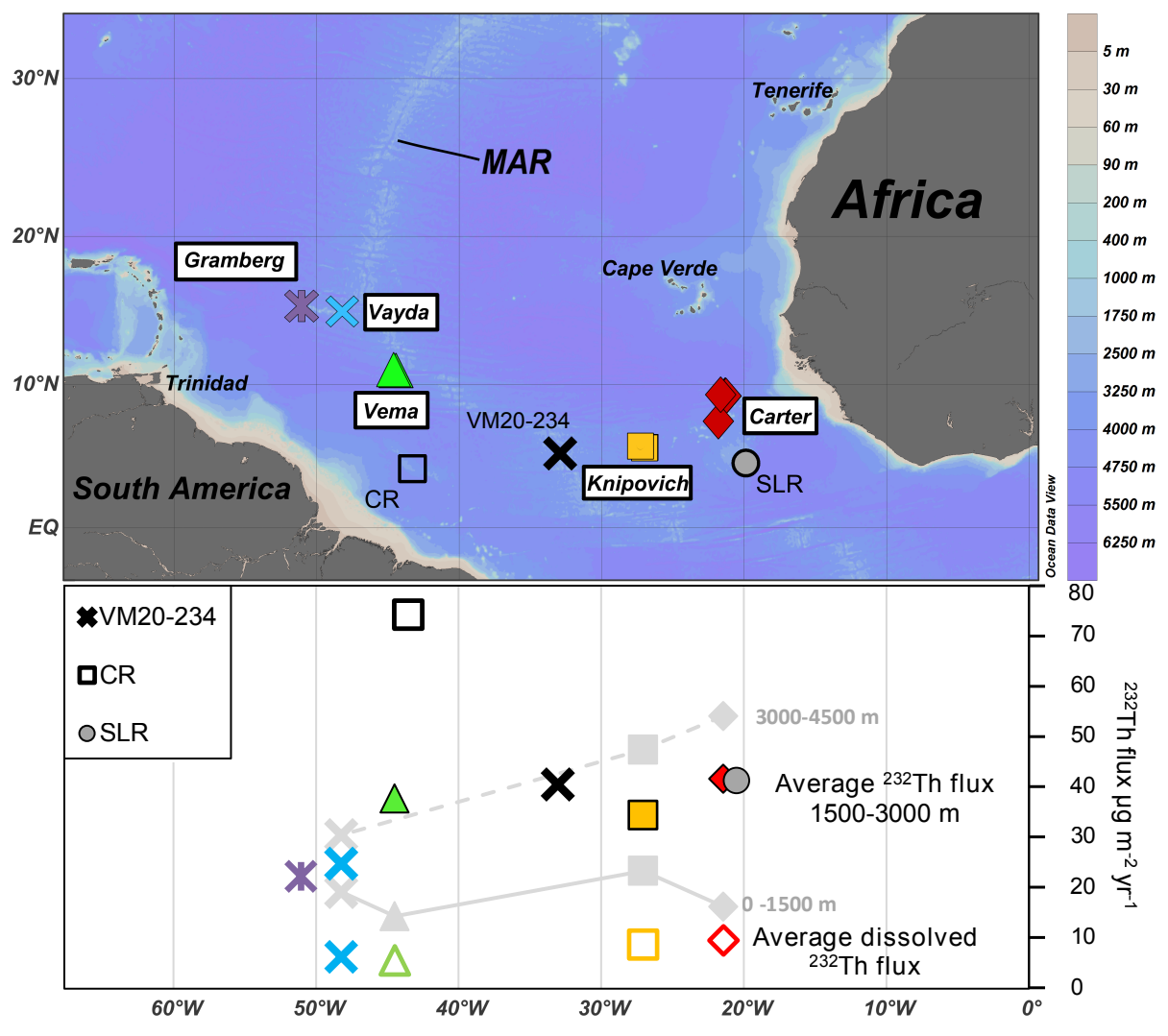


Figure 6. Upper panel shows a map of sample sites whilst the lower panel shows total ^{230}Th -normalised ^{232}Th fluxes and dissolved ^{232}Th fluxes. The grey symbols show sedimentary ^{230}Th -normalised ^{232}Th fluxes at each site for the specified depth interval. The solid colour symbols represent sedimentary ^{232}Th fluxes over the depth interval 1500-3000 m, as a best estimate of representative ^{232}Th fluxes for each site. The hollow colour symbols show the average dissolved ^{232}Th fluxes at each location calculated from seawater. CR and SLR show average core-top ^{232}Th fluxes of the three cores at each location (Francois and Bacon, 1991). The core-top ^{232}Th flux from VM20-234 is taken from Williams et al. (2016).

Figure7

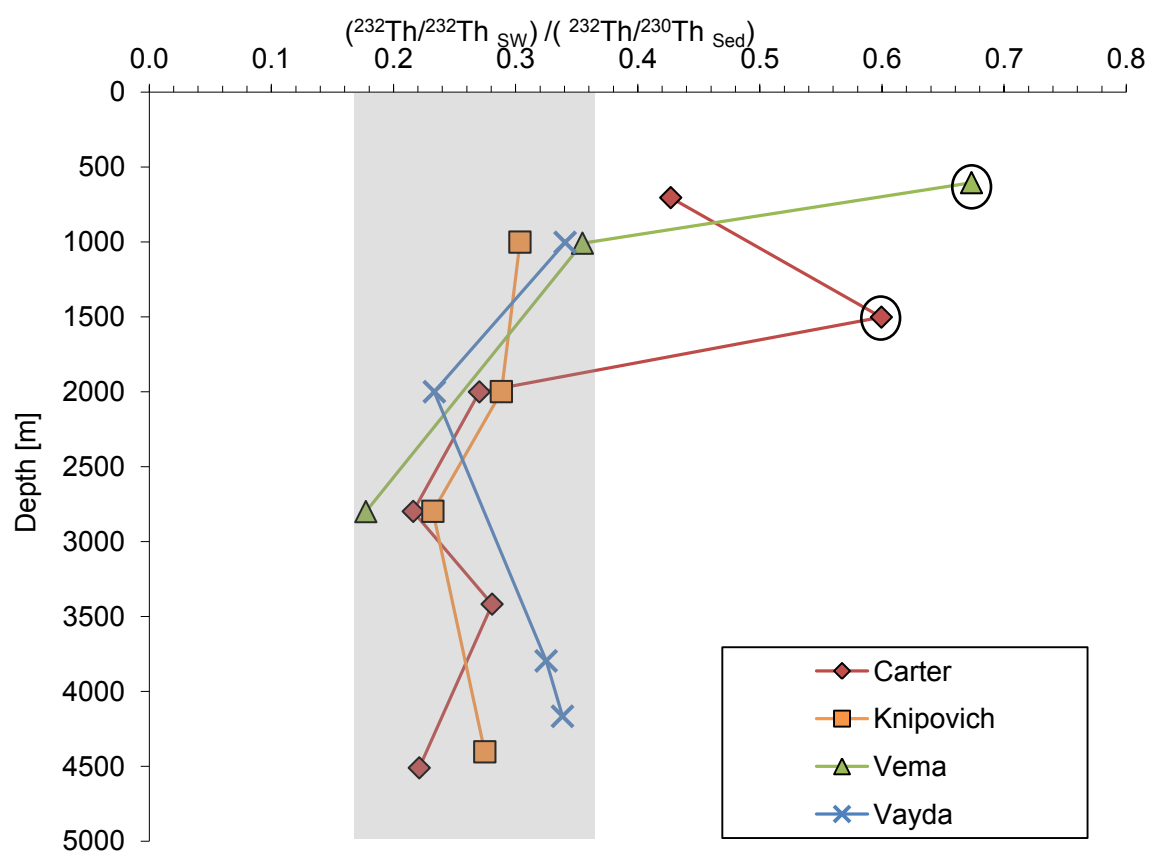


Figure 7. Apparent fractional solubility of ^{232}Th from lithogenic material based on the ratio of seawater and core-top $^{232}\text{Th}/^{230}\text{Th}_{\text{xs}}$ ratios. All but three samples lie within a relatively narrow range (18-35 %) highlighted in grey. The two circled data points are the two points that are excluded from the regression in Figure 5.

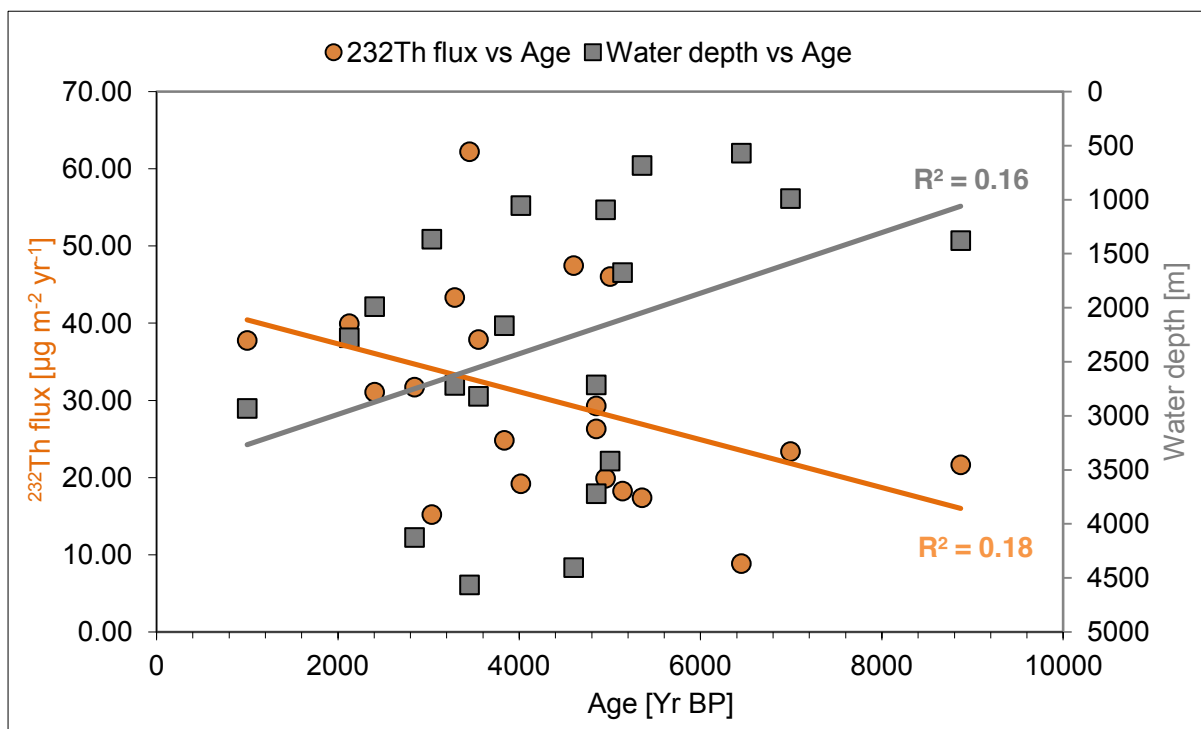


Figure S1. Core-top ages plotted against ^{232}Th flux (orange circles) and water depth (grey squares).

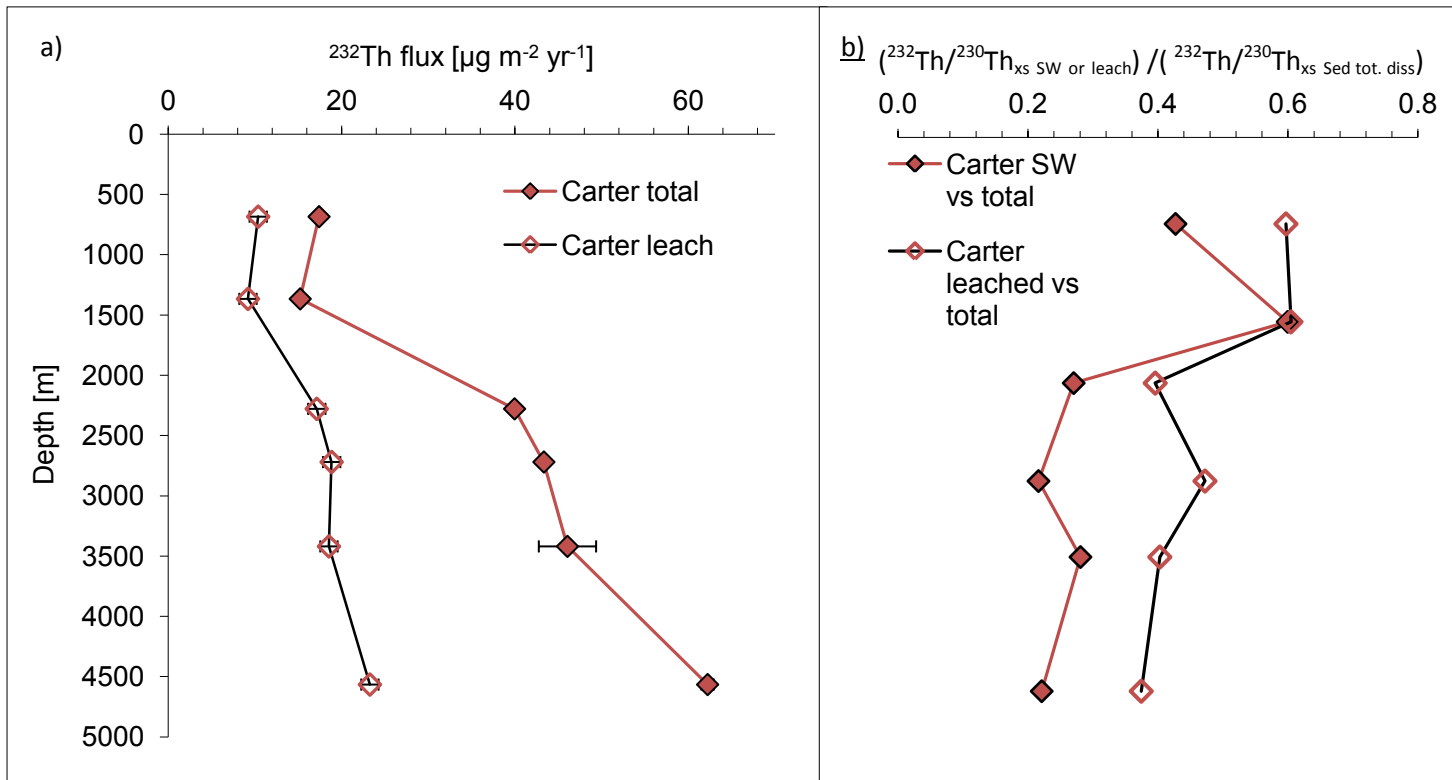


Figure S2. a) Leached (adsorbed) and total ^{232}Th fluxes from the Carter site. b) Comparisons of $^{232}\text{Th}/^{230}\text{Th}_{\text{xs}}$ at Carter between seawater and total sediment dissolutions (solid diamonds) and between sediment leachates and total sediment dissolutions (hollow diamonds).

supplementary information

[Click here to download Electronic Annex: 232Th_230Th GHR et al. Supplement_ Revised.docx](#)

supplementary data

[Click here to download Electronic Annex: 232Th_230Th GHR et al. supplementary_data_Revised.xlsx](#)

Equation1 as PDF

[Click here to download Source or Other Companion File: 232Th_230Th GHR et al. Equation 1.pdf](#)

Equation2 as PDF

[Click here to download Source or Other Companion File: 232Th_230Th GHR et al. Equation 2.pdf](#)

Equation3 as PDF

[Click here to download Source or Other Companion File: 232Th_230Th GHR et al. Equation 3.pdf](#)

Equation 4 revised

[Click here to download Source or Other Companion File: Equation 4 Revised.pdf](#)

Supplement Equation1 as PDF

[Click here to download Source or Other Companion File: 232Th_230Th GHR et al. Equation S1.pdf](#)

Supplement Equation2 as PDF

[Click here to download Source or Other Companion File: 232Th_230Th GHR et al. Equation S2.pdf](#)

Supplement Equation3 as PDF

[Click here to download Source or Other Companion File: 232Th_230Th GHR et al. Equation S3.pdf](#)

Supplement Equation4 as PDF

[Click here to download Source or Other Companion File: 232Th_230Th GHR et al. Equation S4.pdf](#)

Supplement Equation5 as PDF

[Click here to download Source or Other Companion File: 232Th_230Th GHR et al. Equation S5.pdf](#)